

# Tandem Nucleophilic Addition/Diels–Alder Reaction of *N*-Butadienyl *N,O*-Ketene Silyl Acetals with $C_{60}$ : Stereoselective Formation of Bicyclic Octahydroquinolino-1,2,3,4-Tetrahydrobuckminsterfullerenes and Combined NMR Spectroscopic and Computational Evaluation of the Functionalization Reactions

Yves Rubin,<sup>\*,[a]</sup> Padma S. Ganapathi,<sup>[a]</sup> Andreas Franz,<sup>[a,b]</sup> Yi-Zhong An,<sup>[a]</sup> Wenyuan Qian,<sup>[a]</sup> and Reinhard Neier<sup>\*,[b]</sup>

**Abstract:** We have studied the reactivity of the *N,O*-ketene *N*-1,3-butadienyl-*N*-alkyl-*O*-silyl acetals **1a–e** with  $C_{60}$  proceeding through a tandem process to give the adducts **2a–e**. The addition order of these tandem reactions has been evaluated. The initial nucleophilic Michael-like addition of the electron-rich *N,O*-ketene acetal moiety proceeds unusually fast at 25 °C, followed by an intramolecularly accelerated Diels–

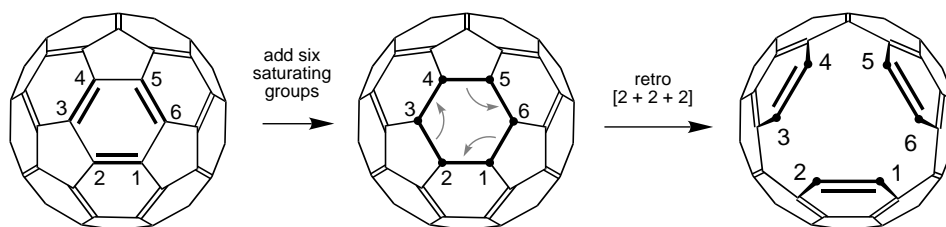
Alder step that is highly diastereoselective. The structures of compounds **2a–e** were determined from the  $^1\text{H}$  and  $^{13}\text{C}$  NMR shifts and from H–H coupling patterns, while their stereochemistry was deduced from 2D T-ROESY NMR experiments. The proposed mechanism for the nucleophilic addition involves single electron transfer followed by radical anion–radical cation recombination. Computational investigations of

the reaction pathways, transition states, and conformational energies have been carried out to corroborate the experimental data.

**Keywords:** cycloadditions • Diels–Alder reactions • electron transfer • fullerenes • semiempirical calculations

## Introduction

We have recently focused our efforts on the regioselective functionalization of  $C_{60}$  at contiguous reactive centers, aiming in particular at additions to the three adjacent C=C bonds within a 6-membered ring to give a fully saturated, planar cyclohexane moiety.<sup>[1, 2]</sup> This venture is particularly challenging because the close proximity of the reactive centers severely hinders the approach of additional reactive moieties



Scheme 1. Spontaneous ring-opening to yield a 1,2,3,4,5,6-hexahydrobuckminsterfullerene.

to these double bonds.<sup>[2, 3]</sup> In spite of this, there is great potential in obtaining designed 1,2,3,4,5,6-hexahydrobuckminsterfullerene derivatives, as they should ring-open spontaneously in a retro [2+2+2] fashion to form a large orifice permitting the introduction of metals into the fullerene cage (Scheme 1).<sup>[2]</sup> This paper explores one pathway to a family of highly congested 1,2,3,4-tetrahydrobuckminsterfullerene derivatives as a preliminary step in our quest for the desired 1,2,3,4,5,6-hexahydro derivatives.

Another reason for developing selective methods for the formation of multiple adducts is that they would provide access to an unprecedented variety of three-dimensional building blocks, potentially useful for physical organic and biological studies. To achieve regioselective additions, the type of reaction and the structure of the addends have to be

[a] Prof. Y. Rubin, Dr. P. S. Ganapathi, Dr. A. Franz, Dr. Y.-Z. An, W. Qian  
Department of Chemistry and Biochemistry  
University of California, Los Angeles  
Los Angeles, CA 90095-1569 (USA)  
Fax: (+1) 310-206-7649  
E-mail: rubin@chem.ucla.edu

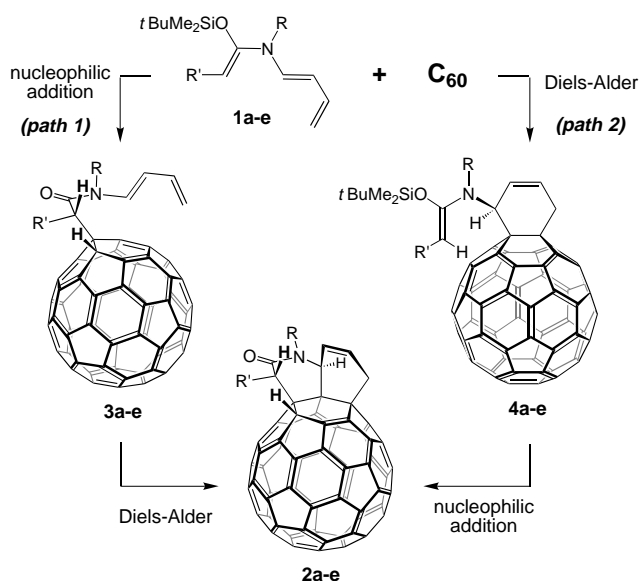
[b] Prof. R. Neier, Dr. A. Franz  
Institut de Chimie, Université de Neuchâtel  
Avenue de Belleveaux 51  
CH-2000 Neuchâtel (Switzerland)

carefully planned. There are now a number of methods to effect the monofunctionalization of  $C_{60}$ .<sup>[4]</sup> However, due to the difficulty of controlling regio- and stereochemistry, multiple additions have been less well studied,<sup>[3–11]</sup> particularly in the case of the sterically biased derivatives of 1,2,3,4-tetrahydrobuckminsterfullerene ( $C_{60}H_4$ ).<sup>[10a, 12]</sup> Interestingly, the distribution of regioisomers in independent bisadditions seems to depend on the type of reaction and is essentially kinetically controlled.<sup>[3, 7]</sup> Tethers separating the two reactive groups have been introduced as a convenient way of directing bisadditions.<sup>[2, 9–11]</sup> The influence of tether structure on the outcome of the bisadditions has been evaluated computationally to the extent possible with the current basis set limits.<sup>[9d, 11a, 13]</sup>

Tandem reactions offer a particularly advantageous and logical way to achieve high regio- and stereoselectivities in cascade (domino), consecutive (isolable intermediates), or sequential reactions (a second component is required to promote an ensuing step), usually with recourse to a diverse array of reacting groups to obtain complex frameworks.<sup>[14]</sup> Tethered bisadditions to  $C_{60}$  can so far be characterized as consecutive tandem reactions by the fact that reactive moieties add at relatively remote double bonds in a stepwise fashion.<sup>[2, 9–11, 14a]</sup> In the tandem reactions using relatively short tethers, highly regio- and stereocontrolled multiple additions to the fullerene framework can be expected to give single products.<sup>[9–11]</sup> This is corroborated by the present study, which is distinguished by the true cascade nature of the process, since the intermediates cannot be isolated.

## Results and Discussion

We were interested in exploring the reactivity of *N,O*-ketene *N*-1,3-butadienyl-*N*-alkyl-*O*-silyl acetals (**1a–e**) with  $C_{60}$  (Scheme 2, Table 1).<sup>[15]</sup> These electron-rich systems were found in earlier work in the Neuchâtel group to undergo fast tandem Diels–Alder/nucleophilic additions with *N*-phenylmaleimide or acryloyl chloride to give the 1,2,3,3a,4,5,5a,6,8a,9-decahydro-



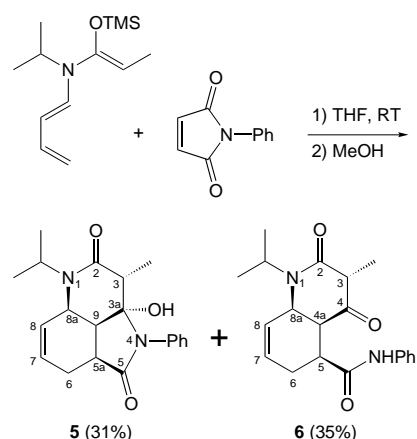
Scheme 2. Tandem reaction of the *N*-dienyl-*N,O*-ketene acetals **1a–e** to  $C_{60}$ .

Table 1. Designation of the substituents in the series of compounds **1–4**, **7**, and **8**.

Suffix	R	R'
<b>a</b>	<i>i</i> Pr	Me
<b>b</b>	PhCH <sub>2</sub>	Me
<b>c</b>	9-Anthryl-CH <sub>2</sub>	Me
<b>d</b>	4-MeOC <sub>6</sub> H <sub>4</sub> CH <sub>2</sub>	4-MeOC <sub>6</sub> H <sub>4</sub>
<b>e</b>	<i>i</i> Pr	CH=CH <sub>2</sub>
<b>f</b> <sup>[a]</sup>	Me	Me

[a] Simplified system used for the calculation section.

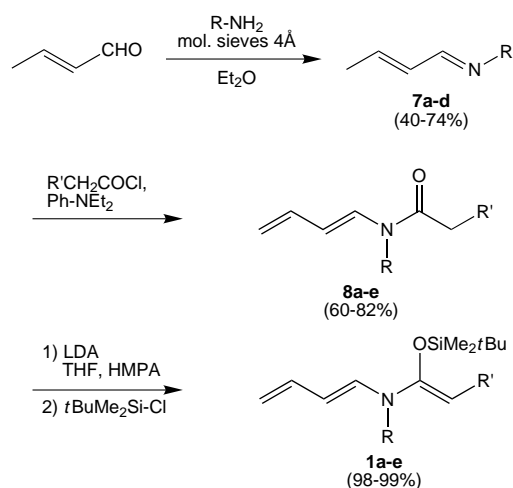
pyrrolo[2,3,4-*de*]quinoline-2,5-dione **5** and the 1,2,3,4,4a,5,6,8a-octahydroquinoline-2,4-dione **6** (Scheme 3).<sup>[16a–c]</sup> Because  $C_{60}$  has a Diels–Alder reactivity similar to that of *N*-phenylmaleimide,<sup>[17]</sup> we expected that the reaction of the *N,O*-ketene



Scheme 3. Tandem reaction of a *N*-dienyl-*N,O*-ketene acetal with *N*-phenylmaleimide.

*N*-1,3-butadienyl-*N*-alkyl-*O*-silyl acetals (**1a–e**) would proceed through path 2 (Scheme 2) involving Diels–Alder addition as the first step to give **4a–e**, followed by a nucleophilic addition to the fullerene to give **2a–e**. We report here that while the tandem reaction indeed produces the desired bicyclic amides **2a–e** in good yields, it follows path 1 by way of intermediates **3a–e** in a surprisingly facile and highly diastereoselective manner.

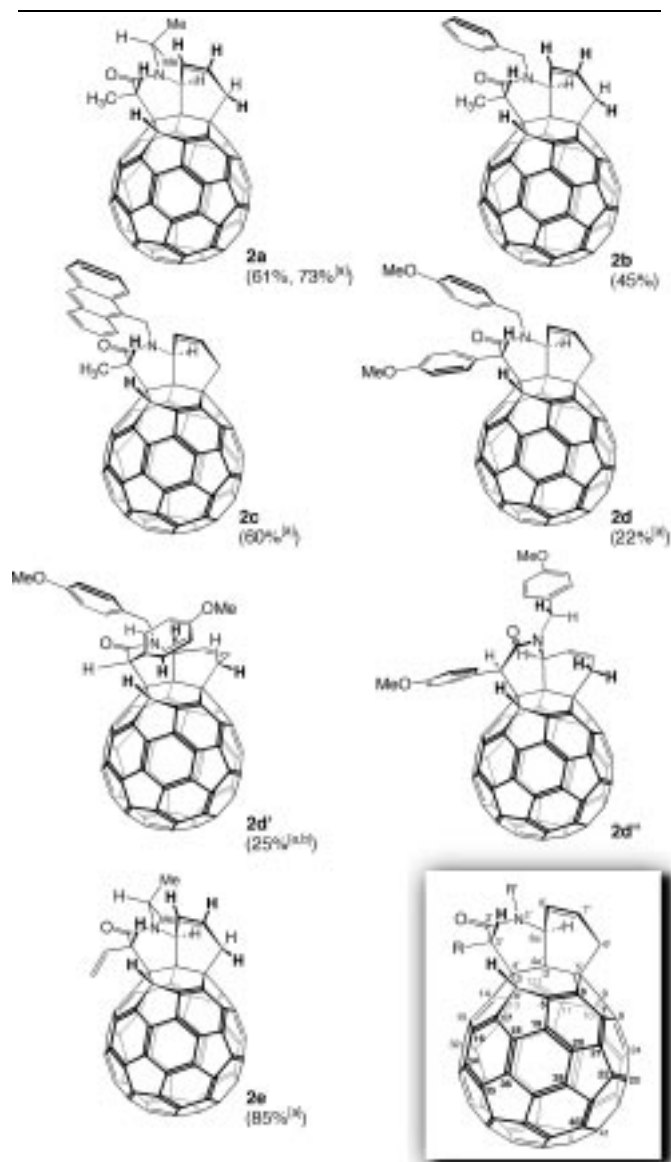
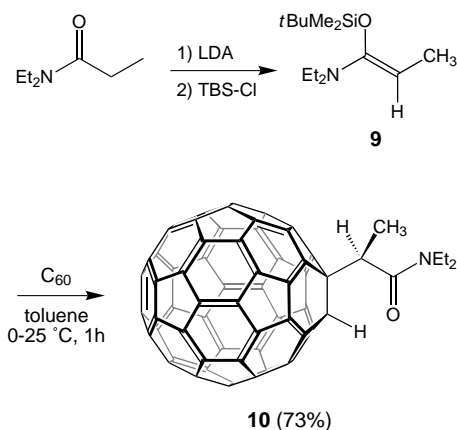
**Preparation of the *N,O*-ketene acetals:** The series of *N,O*-ketene *N*-1,3-butadienyl-*N*-alkyl-*O*-silyl acetals (**1a–e**) were synthesized starting from crotonaldehyde (Scheme 4).<sup>[16]</sup> Condensation with isopropylamine, benzylamine, 4-methoxybenzylamine, or 9-anthrylmethylamine in diethyl ether in the presence of molecular sieves afforded the imines **7a–d** in 40–74% yield. Reaction of these imines with propanoyl, crotonyl, or 4-methoxybenzoyl chloride in the presence of *N,N*-diethylaniline gave the corresponding *N*-alkyl-*N*-butadienyl amides **8a–e** in good yields. Although the silylation of **8a,b** with trimethylsilyl chloride is also feasible,<sup>[16c]</sup> it was much more convenient to prepare the *O*-*tert*-butyldimethylsilyl (TBS) acetals **1a–e** because of their greatly increased hydrolytic stability and ease of formation. Deprotonation of the dienamides **8a–e** with LDA and reaction with *tert*-butyldimethylsilyl chloride afforded the (*Z*)-*N,O*-ketene acetals **1a–e** in high yields.

Scheme 4. Preparation of the *N*-dienyl-*N,O*-ketene acetals **1a–e**.

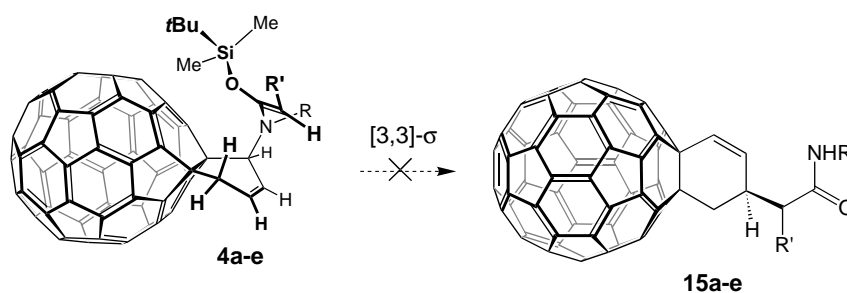
**Tandem reaction of *N,O*-ketene acetals with  $C_{60}$ :** Our initial experiments were performed by syringe addition of the *N,O*-ketene acetals **1a** and **1b** to a solution of  $C_{60}$  in toluene under reflux, which is a condition we have typically used in other Diels–Alder reactions to avoid excessive polymerization of the diene or formation of higher adducts of  $C_{60}$ .<sup>[18]</sup> As will be discussed later, the high temperature (110 °C) is not necessary and the thermal conditions of this reaction can greatly affect its outcome; the *N,O*-ketene acetals **1c** and **1d** gave complex reaction mixtures at these temperatures. In the case of the *N,O*-ketene acetals **1a** and **1b**, the bicyclic adducts **2a** and **2b** were obtained as the only detectable diastereomers in 61 and 45% yields, respectively (Table 2). Carrying out these reactions at 0–25 °C (see below) afforded the adducts **2a** and **2c–2e** in 60–85% yields. These cycloadditions generate a total of six stereocenters with high diastereoselectivity, outlining the potential of the tandem reaction in sterically demanding fullerene functionalizations.

To probe the addition order of these tandem reactions, that is whether the nucleophilic addition precedes the Diels–Alder reaction (path 1, Scheme 2) or vice versa (path 2), a simple silylated *N,O*-ketene acetal **9** of similar steric requirement was prepared from *N,N*-diethylpropionamide (Scheme 5). This compound can add to  $C_{60}$  only in a nucleophilic fashion to give amide **10**. Surprisingly, addition of *N,O*-ketene acetal **9** to  $C_{60}$  occurred extremely easily and cleanly at 0–25 °C, affording amide **10** in 73% yield with no detectable higher addition by-products. This product was identical to the one obtained from the [2+2] photocycloaddition of  $\text{Et}_2\text{N}-\text{C}\equiv\text{C}-\text{CH}_3$  to  $C_{60}$  followed by nucleophilic addition of water to the resulting 4-membered ring enamine and subsequent ring opening as reported by Foote et al.<sup>[19]</sup>

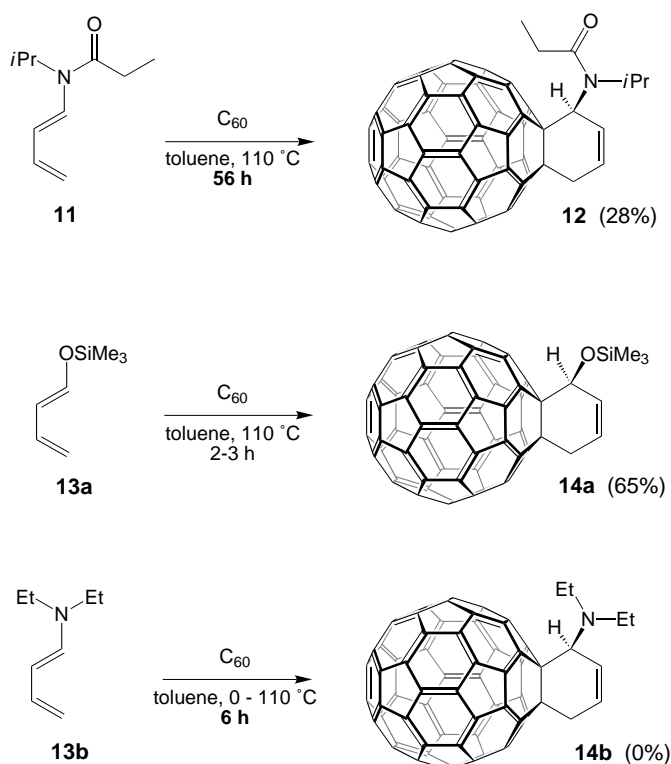
In contrast to the ease of reaction of *N,O*-ketene silyl acetal **9** with  $C_{60}$ , dienamide **11** reacts very slowly to give the Diels–Alder adduct **12** in low yield. However, diene **11** is not electron-rich, since its nitrogen lone pair is delocalized primarily over the amide moiety. Therefore, the relatively electron-rich diene **13a** was used for a better comparison. It does not react with  $C_{60}$  at 25 °C, but addition proceeds

Table 2. Structures of products **2a–e** obtained from the tandem reaction of *N,O*-ketene acetals **1a–e** with  $C_{60}$  and reaction yields. The positional numbering for all compounds described in this study is provided in the boxed structure.[a] Yields for reactions at 25 °C. [b] Yield for 2:1 mixture with **2d**.Scheme 5. Michael addition of model system **9** to  $C_{60}$ .

smoothly at 110 °C in toluene in about 3 h to give **14a** (Scheme 6).<sup>[1, 18c]</sup> By analogy, reaction of Danishefsky's diene with C<sub>60</sub> is reported to occur in 60% yield based on consumed C<sub>60</sub> (PhCH<sub>3</sub>, 110 °C, 4 h) or in 38% isolated yield (PhCH<sub>3</sub>, 45 °C, 15 h).<sup>[17, 18a]</sup> Finally, 1-(*N,N*-diethylamino)butadiene (**13b**) was examined as the



Scheme 7. Potential Claisen rearrangement of intermediates **4a–e**.



Scheme 6. Diels–Alder reaction of model systems **11** and **13a/b** with C<sub>60</sub>.

system most comparable electronically to the *N,O*-ketene acetals **1a–e**, but it too reacted very sluggishly at room temperature or on heating to give traces of Michael-like adducts (addition at C-4 terminus of diene moiety), but surprisingly no Diels–Alder product **14b** (10 equiv **13b**, 0–110 °C, toluene).<sup>[20]</sup> These four examples show that the Diels–Alder reactivity of the *N,O*-ketene acetals **1a–e** must be negligible compared to their nucleophilic addition propensity. Therefore, the first step in the tandem reactions is most likely the nucleophilic addition (path 1, Scheme 2). Incidentally, the fact that the mechanism of the tandem reaction proceeds by way of path 1 explains the lack of formation of the [3,3]-sigmatropic rearrangement products **15a–e**, a possibility that was at the origin of the work with regular dienophiles like *N*-phenylmaleimide (**5**; Schemes 3 and 7).<sup>[16a–c, 21]</sup>

In view of the facile addition of *N,O*-ketene silyl acetal **9** with C<sub>60</sub> at 25 °C, we repeated the reaction of the dienyl system **1a** at this lower temperature. We observed that the

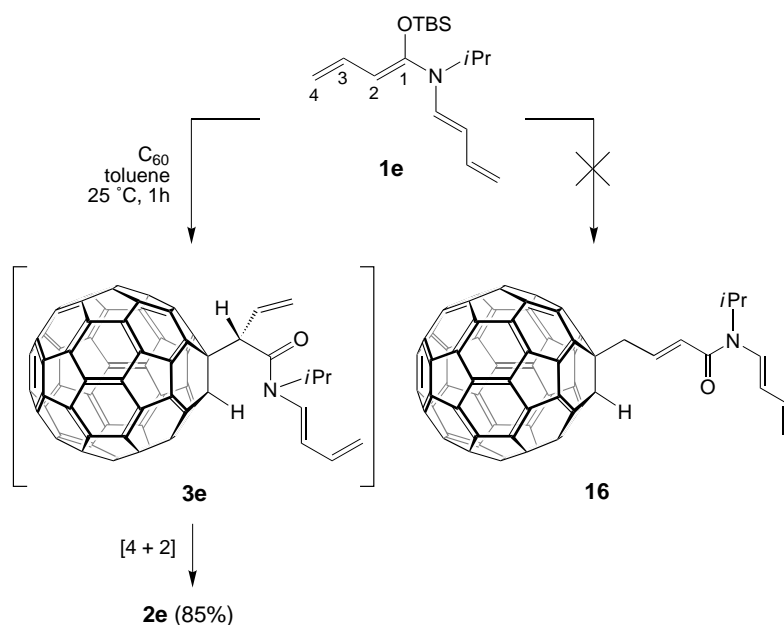
reaction again proceeded very cleanly and that it was completed within 2 h with a substantial improvement in the yield of product **2a** (Table 2). Interestingly, reactions of *N,O*-silyl ketene acetals **1c** and **1d** with C<sub>60</sub> performed in toluene under reflux gave inseparable complex mixtures of products from which the expected bicyclic adducts **2c** and **2d** could be recognized from the crowded <sup>1</sup>H NMR spectra of the crude mixtures. On the other hand, addition of the anthracene derivative **1c** to C<sub>60</sub> at 0 °C followed by stirring at 25 °C gave exclusively the expected bicyclic adduct **2c**. The anthracenyl group of **2c** was not observed to undergo appreciable intra- or intermolecular Diels–Alder reaction with a nearby C<sub>60</sub> double bond (toluene, reflux).

Reaction of the more sterically hindered *N,O*-ketene silyl acetal **1d** with C<sub>60</sub> gave a mixture of the three diastereomers **2d**, **2d'**, and **2d''**. The more polar diastereomer **2d** was obtained pure in 22% yield after column chromatography (toluene/EtOAc 9:1). The less polar fraction was an inseparable mixture of the diastereomers **2d'** and **2d''** in 2:1 ratio (<sup>1</sup>H NMR), which was obtained in 25% yield. Interestingly, in both **2d'** and **2d''** the cyclohexene ring is in an *exo* relationship to the fullerene-attached proton, in contrast to all other compounds prepared in this study, which have an *endo* relationship. Compound **2d''** is the epimer of **2d** at C-3'. In compound **2d'** both the C-3' and C-8a' chiral centers are inverted compared to **2d**. The reduced diastereoselectivity of this reaction could result from the increased steric demand in the Diels–Alder step due to the large *p*-methoxyphenyl group in  $\alpha$ -position of the carbonyl group (Scheme 2, path 1, structure **3d**). However, after the 2:1 mixture of **2d'** and **2d''** had been heated to 75 °C and then cooled to 25 °C in a <sup>1</sup>H NMR experiment, the ratio was changed in favor of the lower energy isomer **2d'** (2:3). This indicates that the nucleophilic step is reversible in this benzylic system at relatively low temperatures and that isomers may form as a result of equilibration during the reaction.

Reaction of **1e** with C<sub>60</sub> gave the single allylic diastereomer **2e** in 85% yield. The nucleophilic addition of **1e** occurred at the 2-position of the ketene acetal dienyl group rather than at the terminus of the dienyl chain (C-4), which would have given compound **16** possessing a thermodynamically more favorable conjugated enamide moiety (Scheme 8).

#### Further functionalization of the 1,2,3,4-tetrahydrofullerenes:

In the context of our general ring-opening goal,<sup>[2]</sup> the novel tandem bicyclic products **1a–e** have three contiguous carbons on the C<sub>60</sub> surface locked into place (i.e. C-1, C-2, and C-3,

Scheme 8. Pathways for the addition of **1e** to  $C_{60}$ .

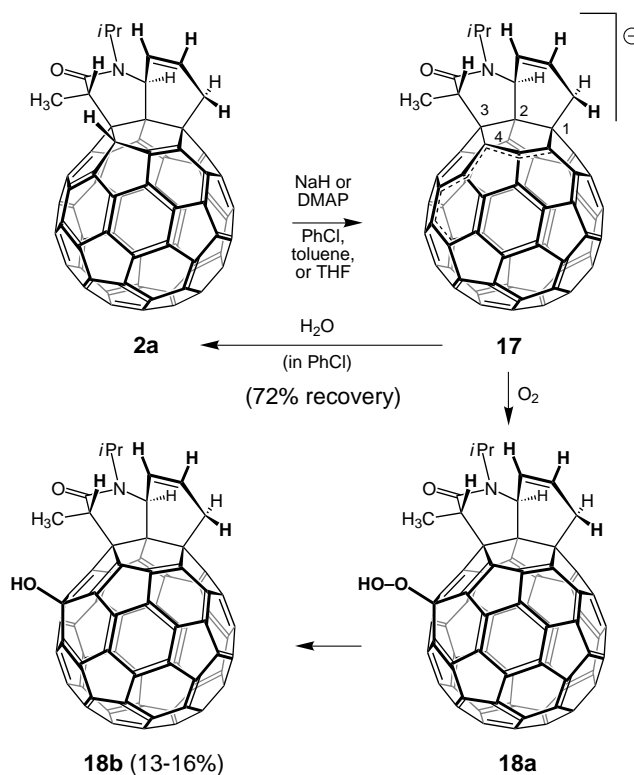
labeling in Table 2). An exploration of effective C–C bond formation reactions was carried out to place a fourth contiguous carbon at C-4 by replacing the labile hydrogen with a C-functional group.

The fullerene-attached proton at C-4 can be removed with NaH in THF or chlorobenzene, giving characteristic dark green solutions of anion **17** and, over time, baseline oligomerization or polymerization products. No ring-opening products involving an intermediate amide enolate (C-3' anion) were observed in the ensuing reactions. These solutions were quenched with water or saturated  $NH_4Cl$  to give either starting material **2a** or the 16-hydroxylated compound **18b** (Scheme 9) depending on the solvent and how carefully the system was deaerated. In THF, compound **18b** was usually obtained preferentially, although considerable loss of material occurred due to the formation of polymers. This reaction was not consistently clean, and minor unidentified, inseparable isomers were also produced. A similar tendency to decomposition was observed with 4-dimethylaminopyridine (DMAP) in THF, giving the product **18b** in low yield (13–16%).<sup>[22]</sup> Deprotonation of **2a** with DBU also gave a green solution in THF but polymers formed very rapidly with complete loss of starting material. Likewise, deprotonation of the 3'-vinylic system **2e** with NaH in THF, which formed the characteristic dark green solution, also afforded the 4-protonated starting material **2e** in quantitative yield. The above results are understandable in terms of the seemingly high reactivity of anion **17** towards traces of oxygen, perhaps by single electron transfer to form superoxide ( $O_2^{\cdot-}$ ) and a fullerene radical.<sup>[23]</sup> Recombination and protonation give **18a**, which is not isolated under the conditions of the experiment. Loss of oxygen from **18a** or a similar peroxide by reduction affords **18b**. If reprotonation of anion **17** occurs instead, **2a** is reformed in preference to other isomers, as supported by the calculations (see below).

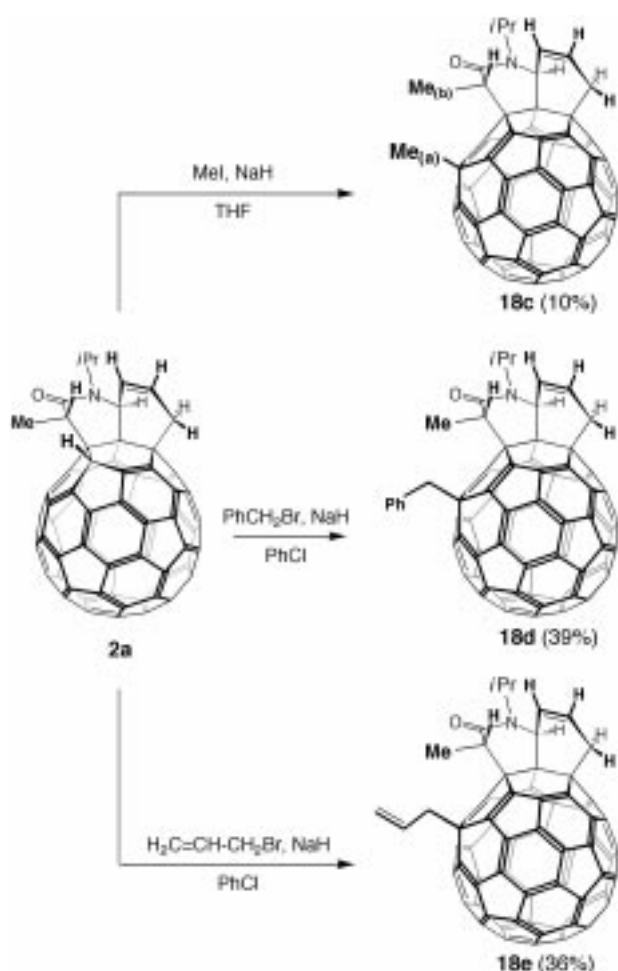
When the nucleophilicity of anion **17** was probed with carbon electrophiles, a selectivity analogous to that of **18b** was

observed. The isopropyl adduct **2a** was treated with an excess of methyl iodide and NaH for 5 h at 25 °C in THF (Scheme 10). Reaction proceeded somewhat poorly in this solvent to give the 16-methylated isomer **18c** in low yield along with polymeric (baseline) material. Reaction occurred exclusively at the 16-position to give this lesser, sterically hindered isomer, as supported by the calculations.

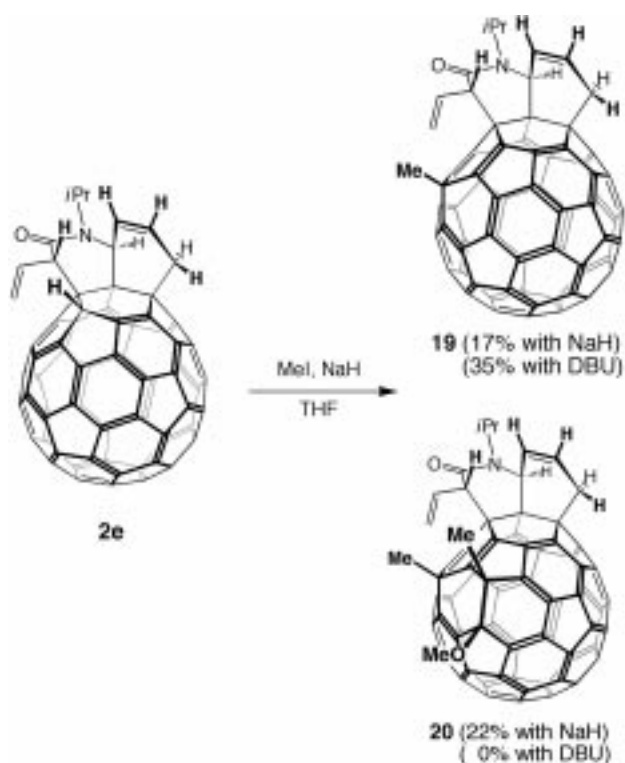
The generality of this reaction was tested with other reactive halides. Reaction of **2a** with NaH followed by quenching of the anion with benzyl bromide gave **18d**, and with allyl bromide the product **18e**

Scheme 9. Deprotonation of compound **2a** and formation of hydroxylated product **18b**.

(Scheme 10). The yields of the reactions were all substantially improved when chlorobenzene was used as the solvent instead of THF. In both cases, a similar site was alkylated which was different from the reprotonation site (**2a**), as was unambiguously established from the 2D T-ROESY spectra (see characterization section) and correlation with calculated HOMO and electron density coefficients (calculation section).

Scheme 10. Alkylation reactions with compound **2a**.

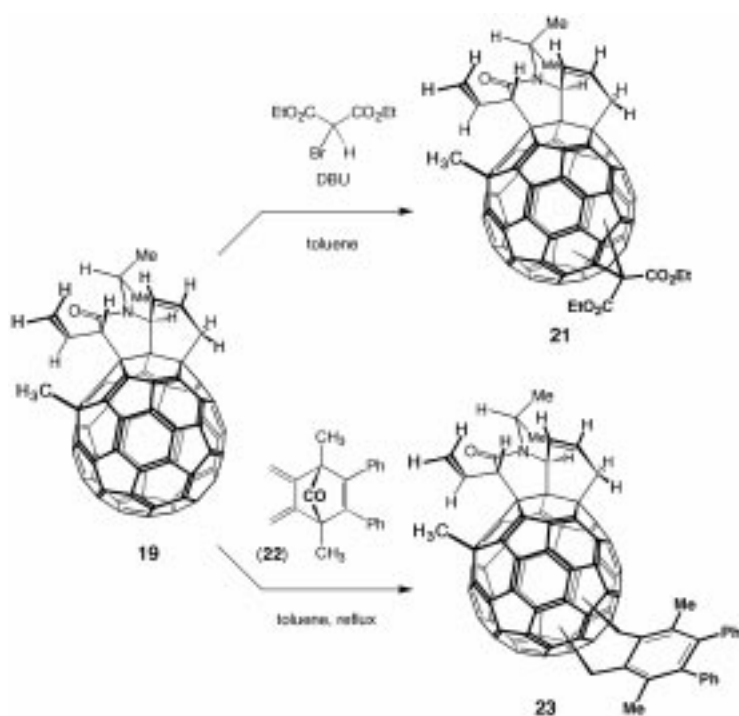
Interestingly, reaction of bicyclic adduct **2e** with NaH and MeI in chlorobenzene gave a mixture of the two products **19** and **20** (Scheme 11). Compound **19** is the 1,3-shifted product similar to **18c**, as demonstrated by the  $^1\text{H}$  NMR and 2D T-ROESY spectra. The slightly more polar product **20** is an interesting doubly methylated/methoxylated compound that results from reaction of **19** with sodium methoxide and subsequent alkylation of the  $\alpha$ -anion with excess MeI. The formation of sodium methoxide in situ can be explained by reaction of NaH with adventitious water ( $\text{NaH} + \text{H}_2\text{O} \rightarrow \text{NaOH} + \text{H}_2$ ) and nucleophilic reaction of hydroxide with MeI to give methanol, which is finally deprotonated. If the reaction was repeated with DBU as the base instead of NaH, only the monomethylated compound **19** was formed in 35% yield. No methylation product resulting from  $\alpha$ -deprotonation of the relatively acidic 3'-proton (allylic amide enolate) was observed. The position of the last-adding methyl and methoxy groups for **20** was assigned based on 2D T-ROESY data (see Figure 10, below) and calculations (Figure 19, below) which show that the 18,36 double bond in **19** has particularly large LUMO coefficients favoring nucleophilic attack at that site. Correlation between LUMO coefficients and regioselectivity explains product distributions in cyclopropanation reactions of  $\text{C}_{60}$  with bromomalonates.<sup>[3]</sup>

Scheme 11. Methylation and methoxy/methylation of compound **2e**.

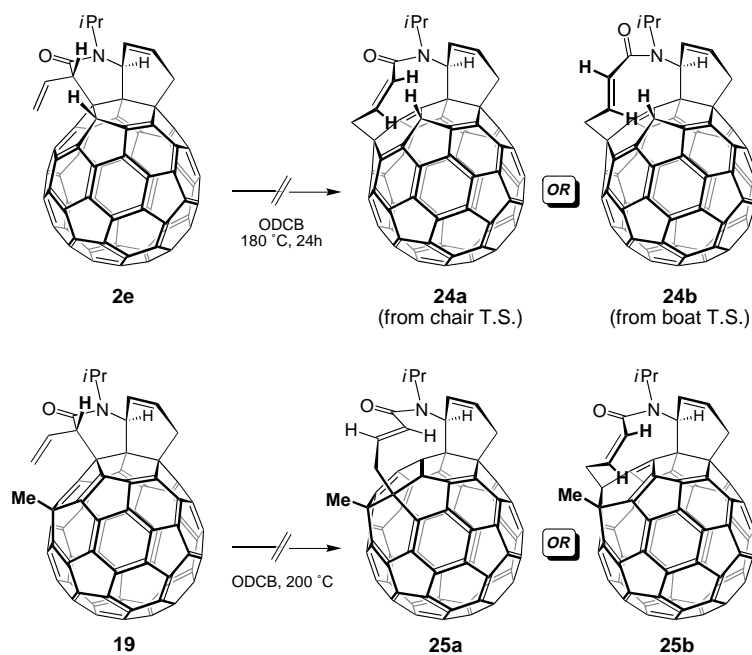
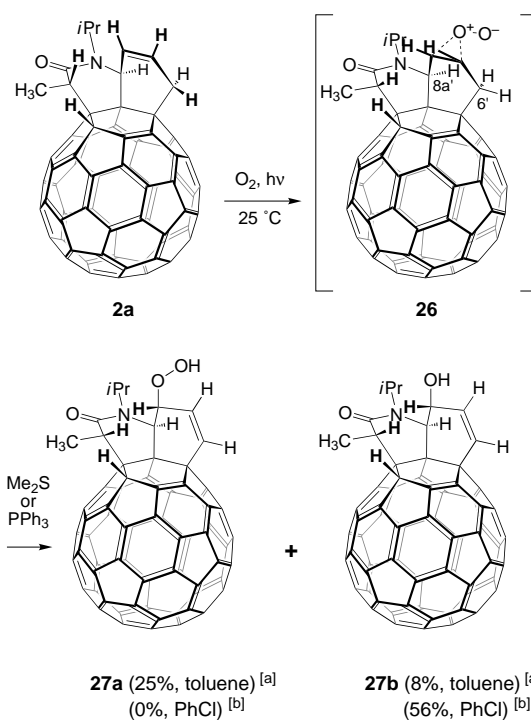
We also tried to take advantage of the clean regioselectivity observed in the formation of compound **20** by reaction of diethyl bromomalonate and compound **19** in the presence of DBU in toluene (the Bingel reaction, Scheme 12).<sup>[3, 24]</sup> Unfortunately, a series of inseparable regioisomeric adducts **21** resulted. This poor selectivity can stem from excessive steric shielding during initial addition of the bromomalonate anion. Similarly, Diels–Alder reaction of diene **22** with compound **19** at  $110^\circ\text{C}$  (Scheme 12) resulted in the formation of numerous less polar spots of regioisomeric adducts **23** (thin layer chromatography,  $\text{SiO}_2$ , toluene/EtOAc 9:1). This aspect of reactivity was therefore not investigated further.

Since adduct **2e** can potentially undergo a [3,3] sigmatropic shift to give interesting and unprecedented Cope rearrangement products (**24a** or **24b**), it was heated up to  $180^\circ\text{C}$  in ODCB in a sealed tube (Scheme 13). However, only the starting material **2e** was recovered even after prolonged heating (24 h); remarkably, absolutely no decomposition occurred during this treatment. The 16-methylated adduct **19** also embodies two Cope systems and therefore we heated it in a sealed tube at  $200^\circ\text{C}$  in the hope of obtaining either **25a** or **25b**. In this case too, only the starting material was recovered along with some decomposition products. The energetics of these reactions are discussed in the calculation section.

The reactivity of the octahydroquinolinone moiety in **2a** was also explored to some extent. For example, we have shown that singlet oxygen ( $^1\text{O}_2$ ) can effectively introduce an allylic alcohol functionality onto a wide variety of cyclohexene-fused fullerenes by the ene reaction.<sup>[18a,d]</sup> Therefore, reaction of compound **2a** with  $^1\text{O}_2$  was carried out using the

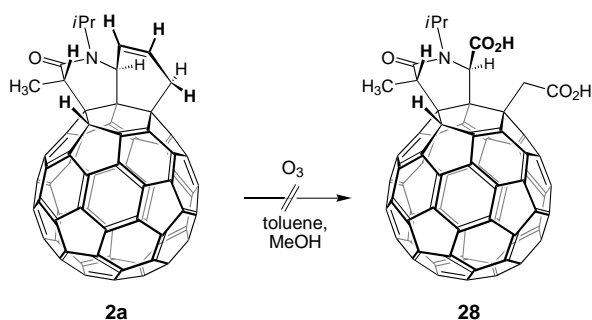
Scheme 12. Further functionalization of compound **19**.

fullerene  $\pi$  system of this compound as the sensitizer (Scheme 14).<sup>[18d]</sup> In toluene, the reaction was complicated by the precipitation of products, which gave a messy mixture upon subsequent reduction with  $\text{Ph}_3\text{P}$  in THF. Milder reduction with dimethyl sulfide was slow and afforded the separable hydroperoxide **27a** and the allylic alcohol **27b** in low yields. When the reaction was carried out in chlorobenzene instead of toluene, the reaction proceeded cleanly to give, after  $\text{Ph}_3\text{P}$  treatment, the allylic alcohol **27b** in good

Scheme 13. Attempted Cope rearrangement of compounds **2e** and **19**.Scheme 14. Singlet oxygen ene reaction with compound **2a**. [a] Reduction with  $\text{Me}_2\text{S}$  or  $\text{Ph}_3\text{P}$  led to polymers in toluene; [b] reduction with  $\text{Ph}_3\text{P}$ .

yield. As can be expected from the *endo* configuration of the cyclohexene double bond, the approach by  $^1\text{O}_2$  occurs from the *exo* side to give the peroxide transition state **26**,<sup>[18a,d]</sup> resulting in the abstraction of the *exo* secondary allylic hydrogen at C-6'. The tertiary allylic proton at C-8a' is not abstracted, presumably because its electrophilicity is diminished by the  $\alpha$ -nitrogen atom. Similar ene reaction with *N*-phenyl-1,2,4-triazoline-3,5-dione<sup>[25]</sup> was attempted, but only decomposition products were formed in this case.

Finally, we were interested in oxidatively cleaving the cyclohexene double bond of **2a** because the resulting dicarboxylic acid **28** could lead to biologically relevant dipeptide/amide derivatives by condensation with amino acids (Scheme 15). However, as we have found several times with other  $\text{C}_{60}$  derivatives,<sup>[2c]</sup> ozone rapidly destroys these compounds at  $-78^\circ\text{C}$  to give highly polar baseline material, even on careful dropwise addition of a cold, dilute solution of  $\text{O}_3$  in methanol into dilute solutions of **2a**. Osmylation reactions<sup>[26]</sup> on this or simpler fullerocyclohexenes (e.g. **14a**) led to complex mixtures most likely resulting from concomitant  $\text{OsO}_4$  addition to the  $\text{C}_{60}$  double bonds.



Scheme 15. Attempted formation of dicarboxylic acid **28**.

### Structural characterization of the products

**Octahydroquinolinone derivatives 2a–e:** The structural connectivities of the octahydroquinolinone derivatives **2a–e**, as well as the related structures **18b–e**, **19**, and **20**, could be readily recognized from their proton and carbon NMR spectra. In determining coupling constants, the fact that signals for the allylic and vinylic protons in the cyclohexene ring have “deceptively simple” coupling patterns<sup>[27]</sup> in most of the compounds made it more difficult to determine coupling constants and required spectral simulation. This task was facilitated by finding that compound **18b** has clean first-order coupling patterns leading to straightforward assignments.

The <sup>1</sup>H NMR spectrum of compound **2b** (Figure 1) is a typical example for the coupling patterns observed in this series of compounds: the olefinic protons H<sub>c</sub> and H<sub>d</sub> appear at δ = 6.86 (ddt) and 6.75 (dt), respectively. The methylene protons H<sub>a</sub> and H<sub>b</sub> of the cyclohexene ring appear as an AB-like pattern at δ = 3.91 (dd) and 3.79 (dq), respectively. The H<sub>e</sub> proton at the bicyclic ring junction appears as a deceptively simple quartet at δ = 4.98 with a measured coupling constant of 2.6 Hz corresponding to the average of three underlying coupling constants (3.0, 3.0, and 1.7 Hz).<sup>[27]</sup> The methyl (d) and methine (q, H<sub>f</sub>) protons on the amide ring show the expected splitting patterns and the proton on the C<sub>60</sub> surface

(H<sub>g</sub>) was readily recognized by the sharp singlet at 5.80 ppm.<sup>[12a,d-f, 28, 29]</sup> In the <sup>13</sup>C NMR spectrum, all 56 fullerene sp<sup>2</sup> carbons are accounted for (54 absorptions, with two having double intensity), appearing between δ = 135 and 155 (Figure 2). The remaining six sp<sup>2</sup> carbons at δ = 127.9, 128.6, 129.3, 129.8, 132.6, and 136.4 belong to the phenyl ring and the alkene functionality of the octahydroquinolinone moiety, while the amide carbonyl appears at δ = 170.4. The tetra-addition pattern on C<sub>60</sub> was confirmed by the <sup>13</sup>C NMR spectrum, which exhibits four sp<sup>3</sup> carbons of the C<sub>60</sub> framework at δ = 61.8, 63.1, 63.2, and 67.4. The question of whether the 1,2,3,4- (identical with 3,4,5,6-) or the 2,3,4,5-addition patterns are present can be answered from the mechanism of the addition and the relative energies of the corresponding structures (see calculation section); only the 1,2,3,4-addition pattern reconciles both arguments.

Although the octahydroquinolinone framework is readily deduced from the <sup>1</sup>H and <sup>13</sup>C NMR spectra and the reactivity pattern of the starting materials, the relative position of the

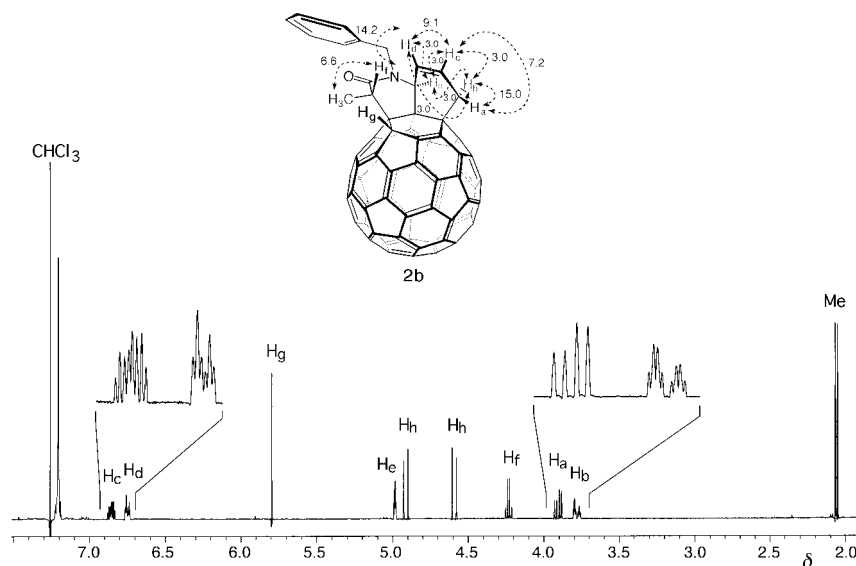


Figure 1. <sup>1</sup>H NMR spectrum of compound **2b** with selected expansions (insets) in CDCl<sub>3</sub>. The spectral resolution was enhanced by Gaussian multiplication of the FID. Apparent proton–proton coupling constants (Hz) are as indicated in the structure.

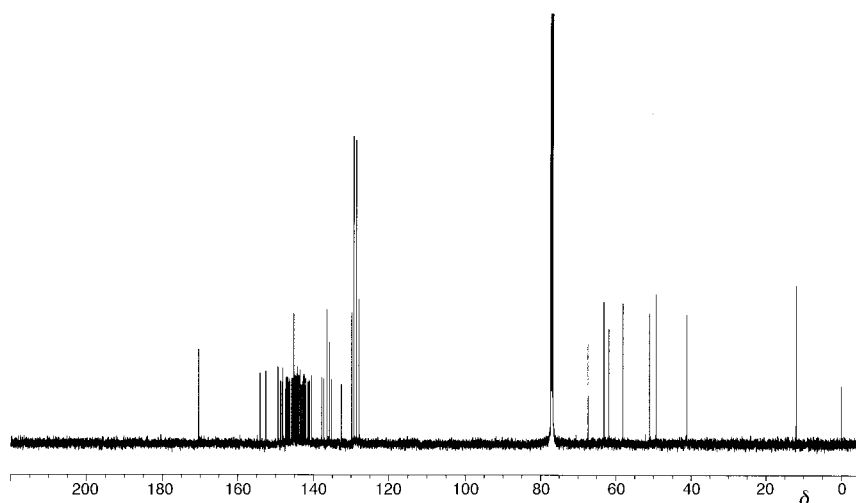


Figure 2. <sup>13</sup>C NMR spectrum of compound **2b** in CDCl<sub>3</sub>.

$C_{60}$ -attached proton ( $H_g$ ) and the relative stereochemistry at the two *exohedral* chiral centers was not deducible from these data. We have previously used the 2D T-ROESY NMR experiment to elucidate stereorelationships of  $C_{60}$  addends.<sup>[30, 31]</sup> The 2D NOESY experiment has been generally less suitable because the mid-range molecular weights of  $C_{60}$  derivatives make them fall into the tumbling rate corresponding to near-zero NOE signals. In the context of this study, complete structural elucidation was obtained with a 2D T-ROESY NMR experiment on **2b**, which clearly shows that the  $C_{60}$  proton ( $H_g$ ) at  $\delta = 5.80$  is attached at the 4-position of the 1,2,3,4-tetrasubstituted buckminsterfullerene framework as evidenced by the strong interactions it exhibits with both the methine proton  $H_f$  and the C-3' methyl group (Figures 3

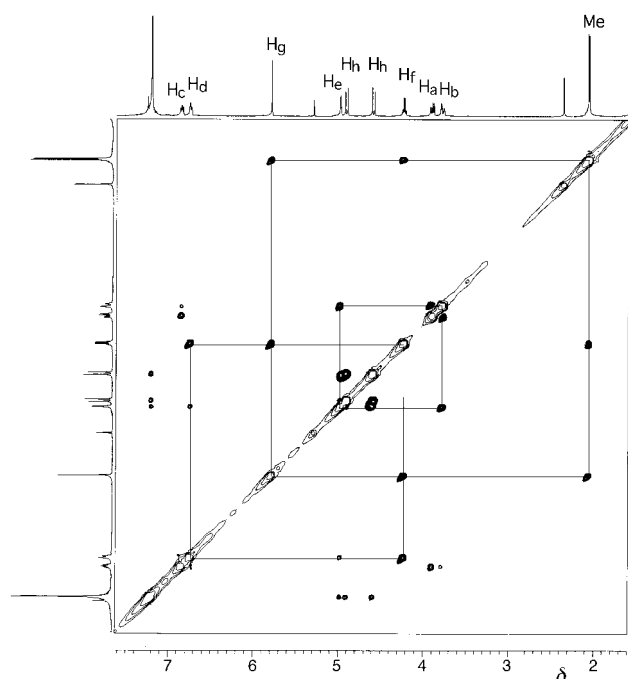


Figure 3. 2D T-ROESY NMR spectrum of compound **2b** in  $CDCl_3$ . Relevant NOE relationships are shown by boxed cross-peaks.

and 4). The relative configuration at the octahydroquinoline bicyclic bridgehead  $8a'$  carbon was deduced from the strong interaction of the proton  $H_e$  with methylene proton  $H_b$ , as well as that of  $H_f$  with  $H_d$ . Thus, the stereochemical structure of **2b** was unambiguously established.

In the 1D proton and the 2D T-ROESY NMR experiments, only one of the two possible conformers (e.g., **2b** (*endo*) but not **2b** (*exo*), Figure 4) is observed. A variable temperature  $^1H$  NMR experiment was performed on compound **2a** to see if an equilibrium between the two possible conformers was established. However, no change in the  $^1H$  NMR spectrum could be observed at the temperature range of 40–140 °C ( $Cl_2CD/CDCl_2$ ), or by cooling to  $-25$  °C, at which temperature the compound precipitates out.

The  $^1H$  NMR,  $^{13}C$  NMR, and 2D T-ROESY spectra of compounds **2a**, **2c**, and **2e** also show correlation patterns that are similar to that of **2b**, establishing the identical connectivity and stereochemistry for all four systems. The relative configuration of **2d** was determined on the basis of the interactions

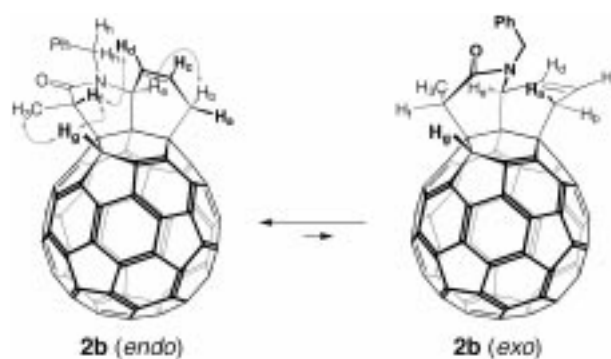


Figure 4. The two possible conformations of **2b** (*endo/exo*) with respect to the alkene bridge) and relevant interactions found in the 2D T-ROESY experiment.

in the 2D T-ROESY spectrum, which are similar to those of compounds **2a–c** and **2e** (Figure 5). From the  $^1H$  NMR spectrum and the interactions of protons in the 2D T-ROESY spectrum of the inseparable mixture of **2d'** and **2d''** (see Supporting Information), it is clear that one of the diastereomers is compound **2d'** as revealed by the strong interactions

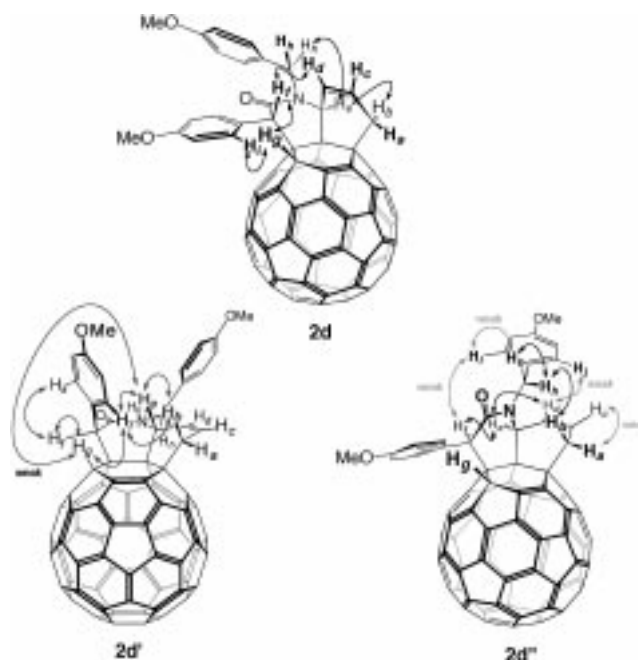
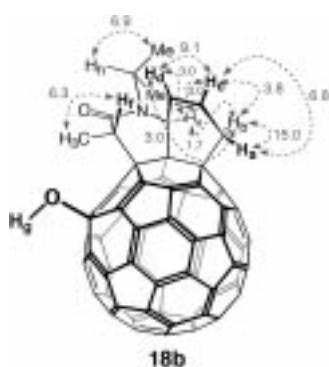


Figure 5. Structures of the diastereomers **2d**, **2d'**, and **2d''** and relevant interactions observed in the 2D T-ROESY experiments.

of protons  $H_f$  with  $H_g$ ,  $H_g$  with  $H_i$ ,  $H_j$  with  $H_b$  and  $H_c$  (strong), and  $H_e$  with  $H_b$ . The other (minor) diastereomer in the mixture is assigned structure **2d''** on the basis of a relatively small number of strong interactions, namely those of protons  $H_e$  with  $H_f$  (very strong) and  $H_b$  with  $H_h$  in the 2D T-ROESY spectrum. In particular, the interaction between  $H_b$  (axial) and  $H_e$  (equatorial) is clearly missing, unlike in compounds **2d** and **2d'**, in addition to which the large coupling constant between  $H_e$  and  $H_d$  (7.1 Hz) further indicates that  $H_e$  is equatorial. Interestingly,  $H_e$  has a quite dramatic spread of chemical shifts between the three compounds (**2d**, **2d'** and **2d''**): it appears at  $\delta = 5.09$  in **2d** and 4.70 in **2d''**, but is

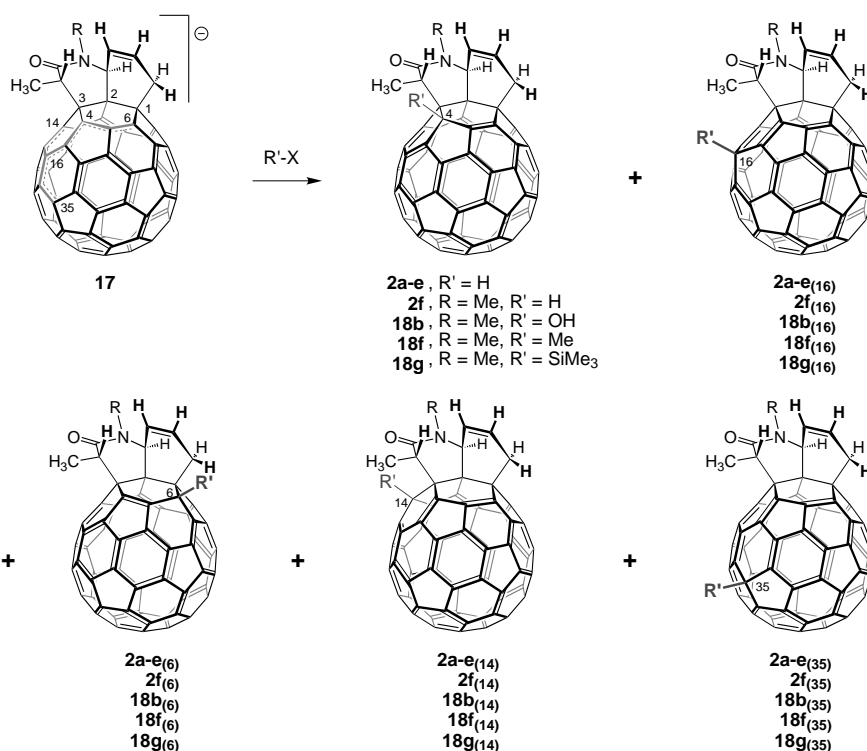
strongly deshielded to  $\delta = 6.25$  in **2d'**, most likely by the *p*-methoxyphenyl group hovering above it.

**16-Hydroxylated or 16-alkylated compounds 18b, 18c–e, 19, and 20:** Since electrophiles can add to anion **17** in at least five positions (Scheme 16) according to the calculated charge densities (vide infra), the question of determining the precise location of the hydroxy or alkyl groups in compounds **18b**, **18c–e**, and **19** had to be answered unequivocally. The curvature of the  $\pi$  framework of  $C_{60}$  tends to localize electrons near  $sp^3$  centers for both anions<sup>[28a,c,e, 32]</sup> and radicals<sup>[33]</sup> (Scheme 16). In analyzing the outcome of these reactions, the two allylic resonance structures of anion **17** with the negative charge localized at C-6 and C-16 were considered significant possible contributors for reaction at these sites. In addition, two pentadienyl resonance structures locating significant amounts of negative charge at the 14- and 35-positions could also cause alkylation at those positions (see calculation section). These five possibilities introduce a difficulty into the  $^1H$  and  $^{13}C$  NMR characterization of the products because they are all asymmetric ( $C_1$  symmetry). The connectivities of the carbons can be assigned with 2D INADEQUATE or C–C HOHAHA techniques,<sup>[26]</sup> but this would have been prohibitively expensive at the time of a large part of this work.<sup>[34]</sup> Fortunately, proton–proton close-contact correlations revealed by 2D T-ROESY  $^1H$  NMR experiments



are well suited for the distinction of the three most probable products (1,2,3,4-, 1,2,3,6-, and 1,2,3,16-isomers) resulting from the protonation, oxygenation, or alkylation of anion **17**.

Initially, the structure of the hydroxylated product **18b** was taken as that of the 16-protonated compound **2a**<sub>(16)</sub> (Scheme 16). The  $^1H$  NMR spectrum exhibits a sharp singlet at  $\delta = 3.92$  in  $CDCl_3$  ( $\delta = 3.82$  in  $CDCl_3/C_6D_6/CS_2$  1:1:2). It is strongly shifted upfield by  $\sim 2$  ppm with respect to the fullerene proton of compound **2a** ( $\delta = 5.82$  in  $CDCl_3$ ), and to most other protons of hydrofullerenes reported in the literature, although their chemical shifts are somewhat solvent-dependent ( $\delta \sim 5.0–7.2$  ppm).<sup>[12a,d,e, 28a–e, 35]</sup> In  $Cl_2CD/$



Scheme 16. Possible alkylation products of anion **17**.

$CDCl_2$ , the fullerene proton is consistently seen as a broad singlet centered at  $\delta = 4.08$ . This raised our suspicions as to its assignment, which were reinforced by a diagnostic loss of this signal upon H/D exchange in presence of  $D_2O$ . The fullerene-attached proton of compounds **2a–e** does not exchange under these conditions. The mass spectrum of **18b**, obtained only with great difficulty, finally confirmed the presence of an additional oxygen atom in the molecule (FAB-HRMS calcd for  $C_{70}H_{17}NO_2 \cdot H^+$ : 904.1337, found 904.1284). Incidentally, the chemical shift of the exchangeable proton is incompatible with that of a hydroperoxide (OOH); the latter should be strongly deshielded as in **27a** ( $\delta = 11.29$ ). Attempted assignment of the  $sp^3$  carbon at position 16 ( $\delta = 85.42$ ) in a  $^1H–^{13}C$  HMQC 1-bond correlation experiment did not show a crosspeak with the 16 proton, as expected if it is bonded through oxygen.

Structure **18b** retains the basic chemical shifts and H–H coupling patterns of **2a**. The position of the hydroxyl group on the  $C_{60}$  surface was assigned to the 16-position based on the two weak crosspeaks seen between  $O–H_g$  and both the *exo* 3'-methyl group and  $H_f$  in the 2D T-ROESY NMR experiment (Figure 6). A strong crosspeak for  $O–H_g$  with the water peak at  $\delta = 1.65$  supports its exchangeable hydroxylic nature. The  $^{13}C$  NMR spectrum of **18b** showed the expected absorptions of the octahydroquinolinone framework. The four  $sp^3$  carbons on the fullerene skeleton were located at  $\delta = 85.4, 69.5, 65.7,$  and  $63.3$ . The upper value is unusually shifted downfield, which allows its assignment as the carbon bearing the OH group.

The alkylated products **18c–e** all exhibited similar spectral features, and only the example of compound **18e** will be discussed here. The  $^1H$  NMR spectrum of the product **18e**

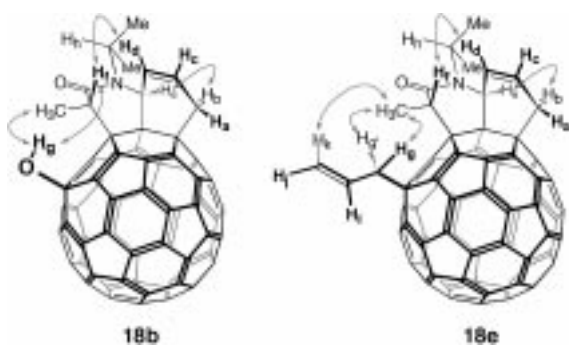


Figure 6. Relevant interactions observed in the 2D T-ROESY experiments for **18b** and **18e**.

showed the disappearance of the  $C_{60}$ -attached proton at  $\delta = 5.82$  in the starting material **2a**, and appearance of the characteristic coupling patterns of the allylic moiety (Figure 7, top trace). The two allylic protons  $H_g$  and  $H_g'$  are observed at  $\delta = 3.51$  and  $3.61$  (both dd) and the vinylic protons appear at  $5.29$  (dd),  $5.33$  (dd), and  $6.34$  (dddd). Otherwise, the spectrum of **18e** retains the basic patterns of **2a**, including the fact that almost no differences in chemical shifts are observed for the protons nearest the affected ring, that is, between  $H_f$  in compound **2a** ( $\delta = 4.18$  in  $Cl_2CD-CDCl_2$ ) and  $H_f$  in product **18e** ( $\delta = 4.20$  in  $CDCl_3$ ), and between the 3'-methyl protons (**2a**,  $\delta = 1.99$ ; **18e**,  $1.97$ ). The fullerene allylation was further confirmed by the presence of an additional  $sp^3$  carbon at  $\delta = 44.5$  and two  $sp^2$  carbons at  $119.8$  and  $132.9$  in the  $^{13}C$  NMR spectrum. The chemical shift of the fullerene carbon bearing the allyl group can be assigned to the signal at  $\delta = 57.9$  on the basis of comparisons with the spectra of **2a** and **18c-e**. As anticipated, the position of the allyl group on the  $C_{60}$  surface was not deducible from the  $^1H$  and  $^{13}C$  NMR data. This was resolved with a 2D T-ROESY NMR experiment which showed a *strong* interaction of  $Me_{(3')}$  with  $H_g$  and  $H_g'$ , but

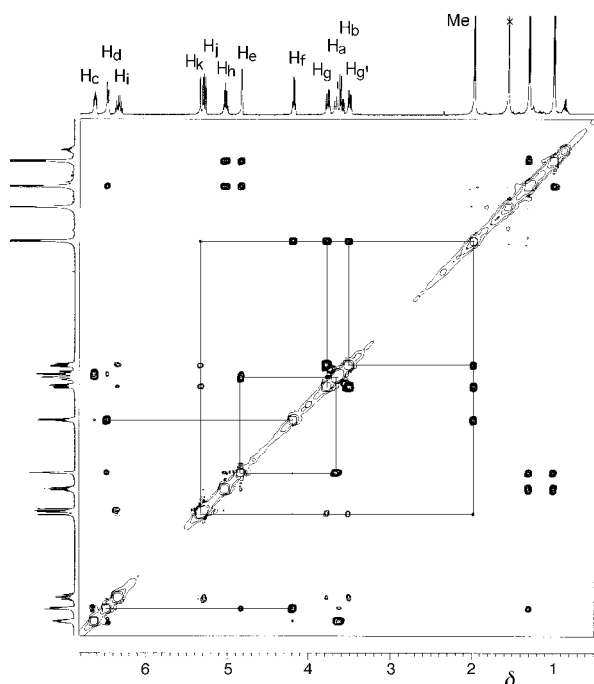


Figure 7. 2D T-ROESY NMR spectrum of compound **18e**.

not  $H_f$  with  $H_g$  and  $H_g'$ , thus clearly indicating that a 1,3-migration had occurred in the alkylation (Figures 6 and 7). These interactions eliminated the possibility of alkylation at positions 4, 6, and 35, which are the most likely other reactive sites for anion **17** (Scheme 16). The other T-ROESY interactions ( $H_d$  and  $H_f$ ,  $H_e$  and  $H_b$ ) were similar to those observed in compound **2a**.

The  $^1H$  NMR spectrum of the methylated vinyl analogue **19** also clearly displays the expected features of its structure (Figure 8, top trace). The characteristic coupling patterns of

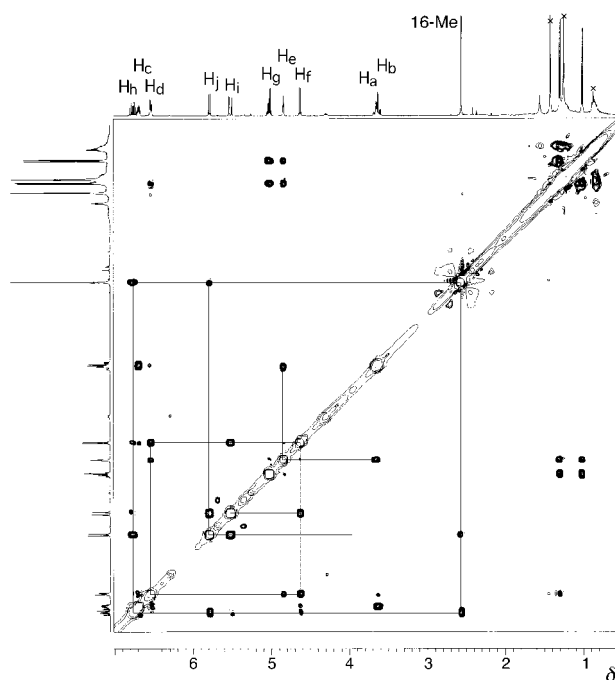


Figure 8. 2D T-ROESY NMR spectrum of compound **19**.

the vinyl group appears at  $\delta = 5.52$  (dd,  $J = 17.3, 1.2$  Hz),  $5.78$  (dd,  $J = 10.0, 1.2$  Hz), and  $6.76$  (ddd,  $J = 17.3, 10.0, 9.4$  Hz), and  $H_f$  is now a doublet at  $\delta = 4.63$  ( $J = 9.4$  Hz). The methyl group at C-16 appears at  $\delta = 2.57$  as a singlet.

The 2D T-ROESY spectrum of **19** is interesting in that it shows strong interactions from the *Z* proton  $H_i$  with  $H_f$ , and of the geminal and *E* protons  $H_h$  and  $H_j$  with the 16-methyl group ( $Me_{(16)}$ , Figures 8 and 9). Furthermore, the large vicinal

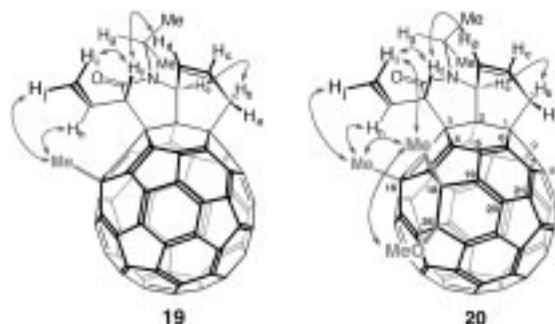


Figure 9. Relevant interactions observed in the 2D T-ROESY experiments for compounds **19** and **20**.

coupling constant observed between  $H_f$  and  $H_h$  (9.4 Hz) correlates with the AM1 calculated  $171.5^\circ$  value for the  $H_f$ -C-C- $H_h$  dihedral angle.<sup>[36]</sup> Thus, the vinyl rotamer shown in Figure 9 is clearly preferred on the averaged NMR time scale. Additionally, the pattern of alkylation at the 16-position is conserved even though the vinyl group is somewhat more sterically demanding than the pseudoequatorial 3'-methyl group in compounds **18c–e**. These observations proved important in assigning the product of methoxymethylation **20** (see below). The other interactions observed for **19** are similar to those in the series **18c–e**.

**Methoxymethylated compound 20:** Because of its surprising formation, the unique product **20**, resulting from nucleophilic addition of methoxide anion to the methylated compound **19**, deserved special attention in its structural investigation. It is particularly perplexing that such high regioselectivity would occur in the addition of methoxide to the C-36 carbon rather than the C-18 or C-21 carbons (vide infra, Figure 19) for a reaction that has shown rather poor selectivity.<sup>[37]</sup> The  $^1\text{H}$  NMR spectrum of **20** displays the same features as that of compound **19**, but additional singlets for the methyl and methoxy groups at  $\delta=2.41$  and  $3.91$  are readily picked out (Figure 10, top trace). The fact that no other compound but

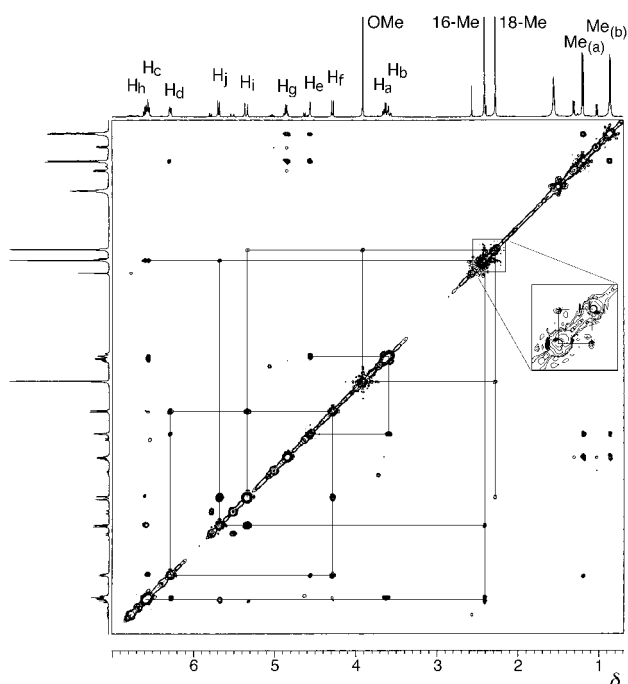


Figure 10. 2D T-ROESY NMR spectrum of compound **20**. The sample contains  $\sim 20\%$  of compound **19** even after careful chromatographic separation.

residual starting material **19** is present in this spectrum, and that no other band moving on the column was observed, speaks for the high selectivity of this reaction. The  $^{13}\text{C}$  NMR spectrum correlates these findings, showing a total of six  $\text{sp}^3$  carbons on  $\text{C}_{60}$ , with the one bearing the OMe group appearing at  $\delta=88.1$ . The additional methyl group  $\text{Me}_{(18)}$  appears at  $\delta=28.2$  ( $\text{Me}_{(16)}$  at 27.3), and the rest of the

spectrum shows little change from the starting material **19** in respect of the fullerene and octahydroquinolinone frameworks.

The regiochemistry of structure **20** was deduced from the significant interaction found in the 2D T-ROESY spectrum between the terminal vinylic hydrogen  $H_i$  and  $\text{Me}_{(18)}$ , which, along with the strong interaction of the *Z* vinylic hydrogen  $H_j$  with  $H_f$ , shows that the additional methyl group is located at or near the 18-position (Figures 9 and 10). Although placing the methyl group at the 4-position would also be in accord with this set of data, the lack of interaction of  $\text{Me}_{(18)}$  with  $H_f$  invalidates this possibility. In support of this deduction, we found the vinyl group to be in the same rotational conformer as that of its predecessor **19** by the interactions of  $H_i$  with  $H_f$  and, on the other side of the double bond, of  $H_h$  and  $H_j$  with  $\text{Me}_{(16)}$ . The fact that the methoxy group shows a significant interaction with  $\text{Me}_{(18)}$  supports its location at the 36-position, also further bolstered by the mechanism of the reaction and the calculations. In addition,  $\text{Me}_{(18)}$  displays a weak interaction with the 1,3-diaxial  $\text{Me}_{(16)}$  (Figure 10, inset), in accord with the distance separating these two methyl groups: In their AM1 minimized geometry, the closest H–H distances are  $2.505 \text{ \AA}$  ( $H_i$ – $\text{Me}_{(18)}$  distance =  $3.016 \text{ \AA}$ ) and  $\sim 1.97 \text{ \AA}$  if the rotations of both methyl groups are taken into account.

**Allylic alcohol 27b:** The ene reaction of singlet oxygen with cyclohexene **2a** is expected to occur from the *exo* face for steric reasons, which facilitates the interpretation of the regio- and stereochemistry of the allylic alcohol product **27b** (Scheme 14). The changes in the allylic patterns between the octahydroquinolinone framework of **2a** and the dodecahydroquinolinone framework of **27b** are immediately apparent in the  $^1\text{H}$  NMR spectrum ( $\text{Cl}_2\text{CD}/\text{CDCl}_2$ ) from the simplification of the vinylic patterns, where  $H_a$  and  $H_b$  appear at  $\delta=6.98$  (dd) and  $6.54$  (dd) (Figure 11, top trace). The

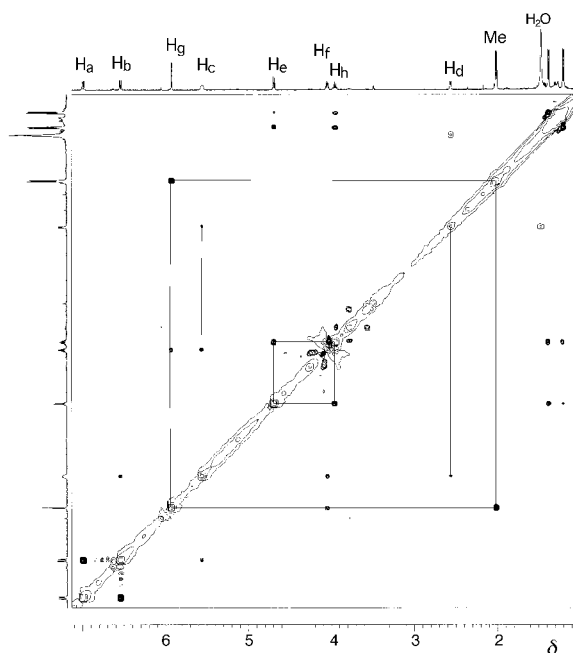


Figure 11. 2D T-ROESY NMR spectrum of compound **27b**.

bicyclic bridgehead proton  $H_c$  also simplifies from a broadened quartet at  $\delta=5.02$  in starting material **2a** to a sharp doublet at 4.70. Also diagnostic is the disappearance of the allylic protons  $H_a$  and  $H_b$  of starting material **2a**, giving rise to a broadened signal at  $\delta=5.56$  (dddd) for the allylic proton  $H_c$  geminal to the hydroxy group. The OH proton is located at  $\delta=2.73$  as a broad singlet. The isopropyl methine septet at  $\delta=4.97$  for **2a** is now shifted upfield to 3.97, perhaps as a result of subtle changes in the conformation of the bicyclic framework or from the presence of the nearby electronegative OH oxygen. The rest of the proton spectrum of **27b** is quite similar to that of **2a**. These features are also readily apparent in the hydroperoxide precursor **27a**, but the OOH proton  $H_d$  appears at  $\delta=11.29$  as a sharp singlet.

It was difficult to obtain the  $^{13}\text{C}$  NMR spectrum of alcohol **27b** in  $[\text{D}_2]$ tetrachloroethane, and impossible for hydroperoxide **27a** for solubility reasons.

The latter was recorded in  $[\text{D}_8]$ tetrahydrofuran. The solvent multiplet centered at  $\delta=2.56$  overlaps the two isopropyl methyl groups of **27a**. The main difference between the  $^{13}\text{C}$  NMR spectra of **27a** and **27b** on the one hand and that of **2a** on the other is the appearance of two prominent vinylic carbon signals at  $\delta=129.0$  and  $135.8$  (for **27a**) and  $129.2$  and  $134.4$  (for **27b**), which, together with the additional presence of the signals at  $\delta=80.1$  (**27a**) and  $72.1$  (**27b**) for the carbons bearing the OOH and OH groups, are diagnostic of their structure.

The stereochemical relationship of the protons in **27a** and **27b** is revealed from their 2D T-ROESY spectra (Figures 11 and 12). Most of the relationships are part of the unchanged "left" side of the molecule, but the diagnostic relationships between  $H_c$  and  $H_f$  in both molecules indicate that the OOH and OH groups are in *exo* relationship to  $H_c$ . Also indicative is the interaction of  $H_c$  with the isopropyl methine proton  $H_h$  in alcohol **27b**, showing as expected that no alteration of the stereochemistry at C-8a' has occurred during the ene reaction.

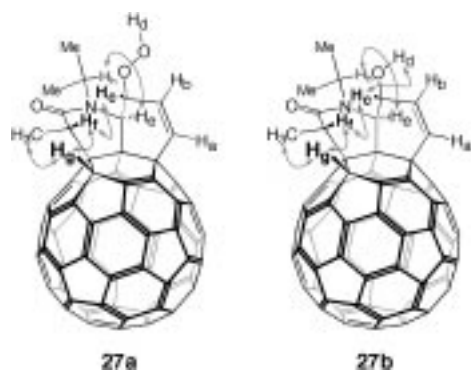


Figure 12. Relevant interactions observed in the 2D T-ROESY experiments for compounds **27a** and **27b**.

**Fast-atom bombardment (FAB) mass spectra:** It is often difficult to obtain good signals for parent ions of fullerene derivatives using various ionization techniques (FAB, LD, MALDI); usually, base peaks for  $\text{C}_{60}$  result with weak parent ions. In this series of compounds, clear resistance to fragmentation of the ionized series **2a–e** and their derivatives was observed. A typical positive ion FAB mass spectrum is shown in Figure 13 for compound **2a**. The  $\text{MH}^+$  parent ion at  $m/z$  888

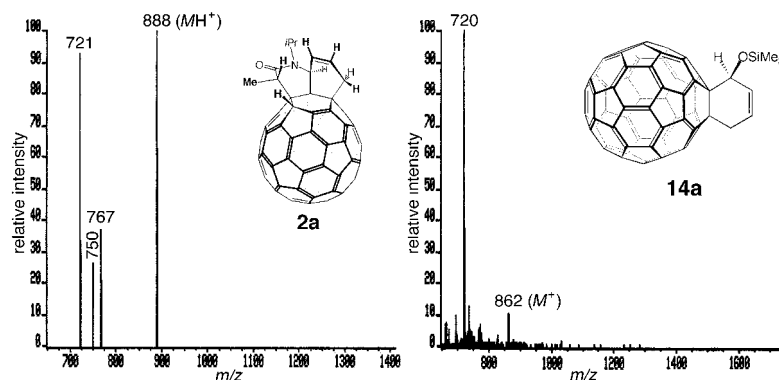


Figure 13. FAB(+)-mass spectra of compounds **2a** and **14a** with *m*-nitrobenzyl alcohol as the matrix.

is the base peak, and fragmentation leads to  $\text{HC}_{60}\text{CHMeOH}\cdot\text{H}^+$  ( $m/z$  767),  $\text{HC}_{60}\text{CHMe}\cdot\text{H}^+$  (750), and  $\text{C}_{60}\cdot\text{H}^+$  (721). On the other hand, the fullerocyclohexene **14a** shows a weak parent ion at  $m/z$  862 and a base peak for  $\text{C}_{60}$  at  $m/z$  720. Even in the case of compounds such as hydroperoxide **27a** and alcohol **27b** with functionalities that normally fragment (OOH, OH), the base peaks are those of the parent ions at  $m/z$  920 ( $\text{MH}^+$  for **27a**) and 903 ( $M^+$  for **27b**). The particular stability of the parent ions in this work allowed facile high-resolution mass spectra to be recorded for all compounds.

**Electronic absorption spectra:** The UV/Vis absorption spectra of the compounds in the series **2a–e** with a 1,2,3,4-tetrahydro addition pattern are all nearly identical, an observation reflected in the uniform dark brown color of their solutions. The UV/Vis spectrum of compound **2a** is represented in Figure 14. With a maximum absorption at 256 nm, the spectrum tails down to 730 nm. A characteristic absorption is observed at 432 nm, together with shoulders at 328 and 404 nm. There are three weak but well-resolved absorptions at 648, 676, and 712 nm. The spectrum of this 1,2,3,4-tetrahydro[60]fullerene does not differ very much from that of a typical 1,2-dihydro[60]fullerene (e.g., compound **14a**) in that the sharp absorption at 432 nm and its associated shoulder at 404 nm lie practically at the same positions compared to the characteristic absorptions at 436 and 410 nm for **14a**.

The UV/Vis absorption spectra for other addition patterns in this work are represented by the 16-methylated and 36-methoxy-16,18-bismethylated derivatives **19** and **20** (Figure 14). These compounds are dark brown in solution, with the former having a greenish hue, and the latter an orange tone. Their spectra show considerable reduction in band

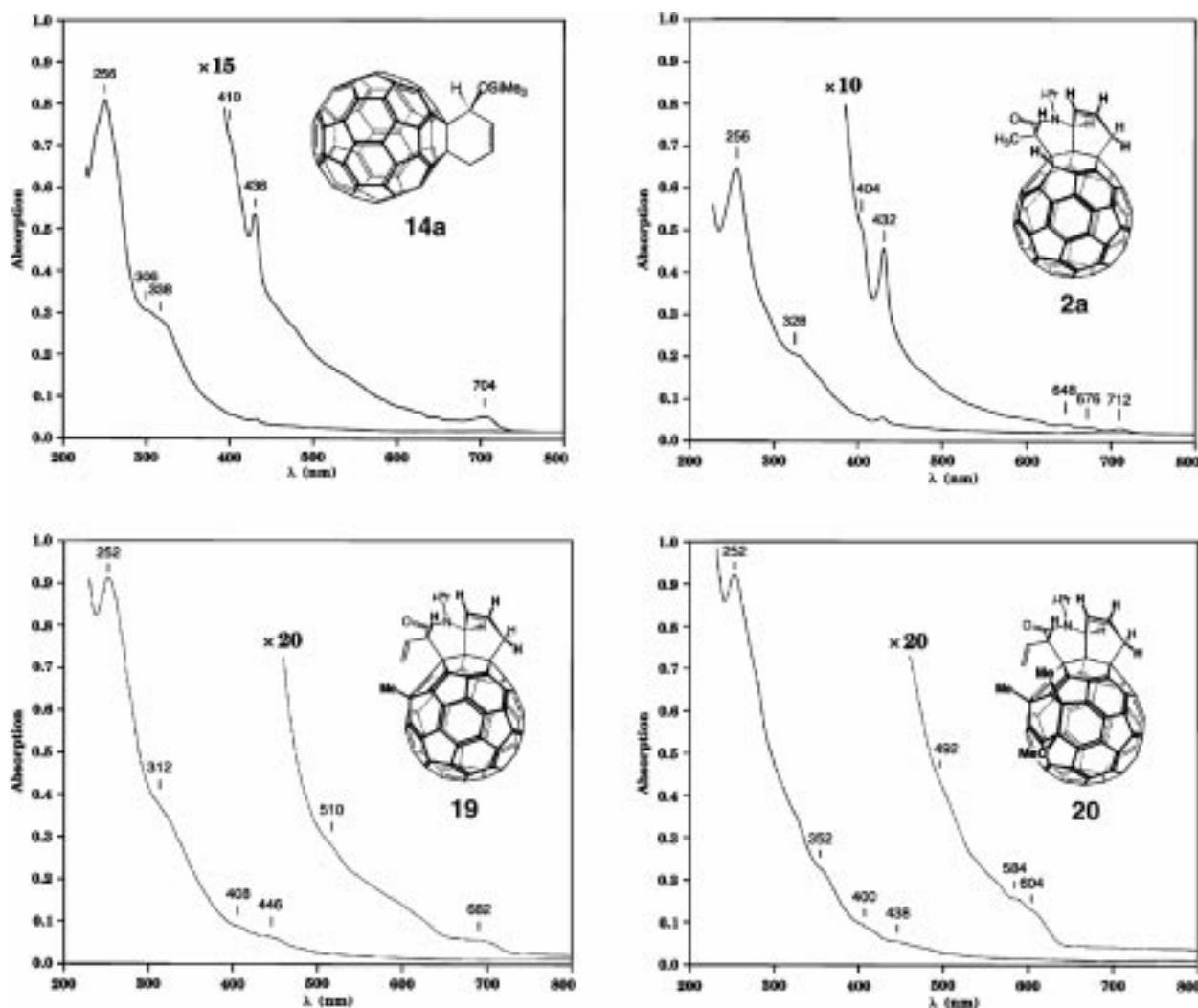
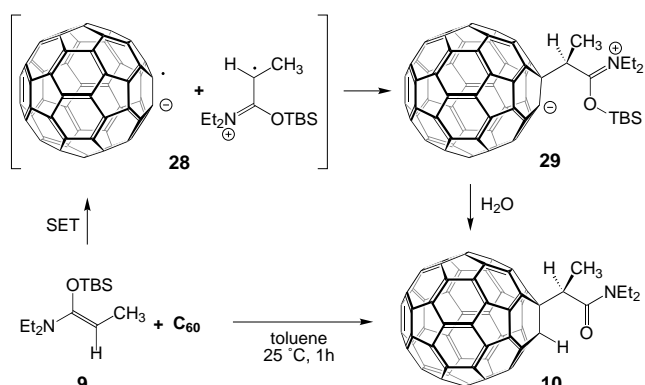


Figure 14. UV/Vis spectra of compounds **2a**, **14a**, **19**, and **20**.

structure, and the absorption of compound **20** tails off much more rapidly at 630 nm than that of its less saturated predecessor **19** (720 nm). Shoulders at 312, 408, 446, 510, and 682 nm are observed for **19**, some of which can be recognized as shifted to the blue (400, 438, 492, and 604 nm) in compound **20**.

**Mechanistic considerations:** The comparative reaction rates for the two partners in the tandem reaction described above show that the nucleophilic addition of **9** to  $C_{60}$  is very fast at 25 °C and even at 0 °C (Scheme 5). This reaction must proceed through a single electron transfer (SET) mechanism involving the zwitterionic intermediates **28** (radical ion pair) and **29** (radical recombination product) as shown in Scheme 17.<sup>[15, 19, 38, 39]</sup> The unusual rate of this reaction at first seemed surprising because analogous additions of *O,O'*-ketene silyl acetals to  $C_{60}$  occur only from their triplet excited state.<sup>[15, 38, 39]</sup> However, although there are no reported one-electron oxidation potentials for *N,O*-ketene acetals available in the literature,<sup>[40]</sup> and no theoretical estimation of these numbers has been performed,<sup>[15a]</sup> the nitrogen atom of the *N,O*-ketene acetals **1a–e** should significantly lower their



Scheme 17. Single-electron transfer mechanism for the Michael addition of **9** to  $C_{60}$ .

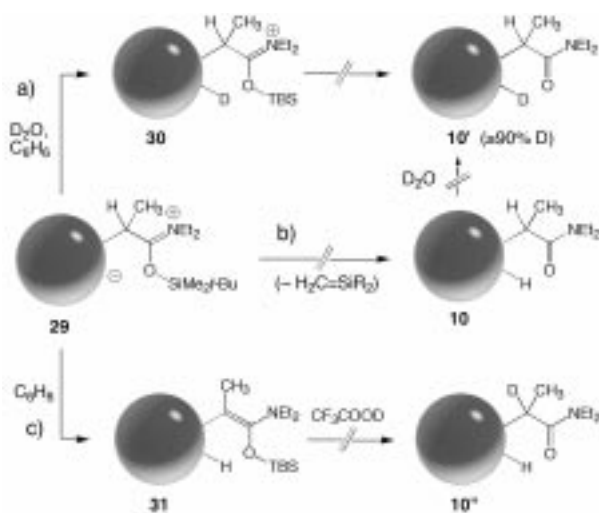
oxidation potentials in comparison to the *O,O'*-ketene silyl acetals, permitting SET through a lowered activation barrier.

As noted earlier, electron-rich systems like Danishefsky's diene or the aminodiene **13b** do not react rapidly with  $C_{60}$  below ~100 °C (Scheme 6). On the other hand, the *N,O*-ketene acetals **1a–e** react as fast as the model system **9**, which supports the precept that the nucleophilic addition occurs

first. Since we have never observed intermediates of type **3a–e**, the intramolecular Diels–Alder step following the formation of amides **3a–e** must occur very easily (i.e., the reaction barrier should be lower than  $10 \text{ kcal mol}^{-1}$ ).<sup>[41]</sup> This is in striking contrast with the poor reactivity displayed by the dienamide **11** (Scheme 6). The intramolecular nature of this reaction must be therefore at the origin of the rate acceleration.<sup>[42]</sup>

The  $\text{H}^+$  source for protonation at the  $\text{C}_{60}$   $\text{sp}^3$  carbanion in the last step of the nucleophilic addition was also investigated. The potential proton sources can vary according to the basicity of anion **29** or its desilylated analogue. The acidity of the  $\text{C}_{60}$ -attached hydrogen of **10** in a polar solvent should be comparable to that of 1,2-*t*Bu $\text{C}_{60}\text{H}$  ( $\text{p}K_{\text{a}} = 5.7$  in DMSO) or  $\text{C}_{60}\text{H}_2$  ( $\text{p}K_{\text{a}(1)} = 4.7$ ,  $\text{p}K_{\text{a}(2)} = 16$  in DMSO), but this would need to be investigated quantitatively in separate study.<sup>[28]</sup> In qualitative terms, Diederich et al. have observed that the acidity of the hydrogen of 1,2-( $\text{Me}_3\text{Si}-\text{C}\equiv\text{C}$ ) $\text{C}_{60}\text{H}$  is strongly dependent on the solvent.<sup>[28c]</sup> In DMSO, deprotonation occurs easily with  $\text{K}_2\text{CO}_3$ ; however, in THF sodium hydride is necessary, and in toluene DBU succeeds but not NaH. A similar observation was made by Meier et al. for the  $D_3$ -symmetric 1,2,33,41,42,50- $\text{C}_{60}\text{H}_6$ , whose acidity seems to be much weaker than that of 1,2-*t*Bu $\text{C}_{60}\text{H}$ ; no exchange is observed with  $\text{D}_2\text{O}$ /toluene for several hours.<sup>[28a]</sup>

Since the basicity of anion **29** or its desilylated analogue is most likely of the order of that of the anions of 1,2-*t*Bu $\text{C}_{60}\text{H}$ ,<sup>[35a]</sup> 1,2-( $\text{Me}_3\text{Si}-\text{C}\equiv\text{C}$ ) $\text{C}_{60}\text{H}$ ,<sup>[28c]</sup> or compounds **2a–e** in the *same* apolar solvent toluene, one can invoke three likely proton sources as shown in Scheme 18: a) the proton is



Scheme 18. Deuteration pathways for intermediate **29**.

coming from adventitious water, b) the proton is abstracted from the silyl group, which affords an unlikely silene, and c) the proton is abstracted by intramolecular transfer from the carbon in the  $\alpha$ -position to the amide functionality in **29** to form intermediate **31**.

To distinguish between these possibilities, the following straightforward tests were performed. First, the reaction of **9** with  $\text{C}_{60}$  was carried out in  $\text{C}_6\text{H}_6$  containing a drop of  $\text{D}_2\text{O}$ . The

product was obtained without workup, giving product **10'** with  $>90\%$  deuterium incorporation at the  $\text{C}_{60}$   $\text{sp}^3$  carbon, as determined by  $^1\text{H}$  NMR integration. This result provides evidence for path a, in which intermediate **29** is rapidly protonated by  $\text{D}_2\text{O}$  to furnish **30**, hydrolyzing to product **10'**. Furthermore, compound **10'** does not exchange its deuterium in a measurable amount ( $^1\text{H}$  NMR) upon chromatography on silica gel ( $\text{PhCH}_3$ ). These results indicate that path b should be excluded, especially since silene formation is very unlikely. Proton transfer from the silyl group should not lead to deuterium incorporation to give **10'**. A slower H/D exchange occurring after initial proton transfer is not likely, because we found that a strong base (NaH) is necessary to deprotonate the  $\text{C}_{60}$ -attached proton (see below). Also, stirring compound **10** with  $\text{D}_2\text{O}$  in THF at  $25^\circ\text{C}$  for 2 h did not lead to detectable H/D exchange.<sup>[28a,c]</sup> Path c can also be ruled out on the basis of the H/D exchange. In any case, this was confirmed further by adding compound **9** to  $\text{C}_{60}$  under rigorously anhydrous conditions in benzene. The reaction mixture was quenched with 99.5%  $\text{CF}_3\text{COOD}$ . No deuterated product **10''** was observed; only compound **10** was formed, as shown by  $^1\text{H}$  NMR. If an intramolecular proton transfer occurred in **29**, the resulting *N,O*-ketene acetal **31** should be hydrolyzed by  $\text{CF}_3\text{COOD}$  to the deuterated product **10''**.

These results indicate that the  $\text{C}_{60}$ -attached proton originates from adventitious water. In fact, addition of a drop of water to the reaction mixture of  $\text{C}_{60}$  and ketene acetals **1a–e** accelerates the tandem reactions and gives slightly higher yields of products **2a–e**. Interestingly, photochemical addition of the analogous *O,O'*-ketene silyl acetals did not lead to any deuterium incorporation when the reaction was carried out in presence of  $\text{D}_2\text{O}$ .<sup>[15a,b]</sup>

## Theoretical calculations

**Methods:** Semiempirical calculations were carried out with Spartan 4.0 (SGI) or MacSpartan Plus (Macintosh). Geometries were optimized at the RHF AM1 semiempirical level. Monte Carlo conformational searches were performed with MacroModel 3.5 using the MM3 force field. For the Diels–Alder transition-state calculations, stationary points were confirmed by vibrational frequency analysis on the fully optimized AM1 structures. To simplify calculations by avoiding substituent rotamers, the *N*-methylated analogues of most of the compounds were used in the calculations, since the reactions with the four different *N*-alkylated systems provided similar experimental results. The numbering suffix for the *N*-methylated analogues used throughout this section is the same as that of Table 1.

## Regioselectivity of the tandem nucleophilic/Diels–Alder

**additions:** The regioselectivity of the tandem reactions is dictated by the order of addition of the two reactive centers on adjacent  $\text{C}=\text{C}$  double bonds of  $\text{C}_{60}$  (*cis*-1 positions).<sup>[3, 4]</sup> However, the differentiation of the 1,2,3,4 and 2,3,4,5-regioisomers that can be formed in principle would not be possible based only on the spectroscopic data (Figure 15). Experimental differentiation between the 1,2,3,4- and 2,3,4,5-addition patterns is only indirect since the products both have

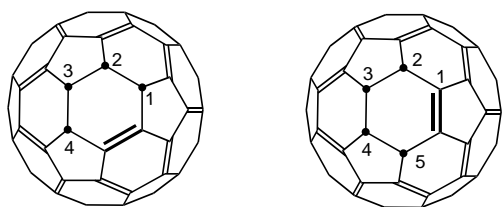


Figure 15. Schematic addend locations for 1,2,3,4- and 2,3,4,5-regioisomers.

$C_1$  symmetry and therefore cannot be distinguished by the number of their  $^{13}\text{C}$  NMR signals. Only  $^{13}\text{C}$ - $^{13}\text{C}$  2D NMR correlation techniques,<sup>[26]</sup> or an X-ray crystallographic analysis, can provide direct proof of the connectivities of these compounds. This is a non-negligible issue, as these problems have the potential to severely hamper further evaluation of functionalization reactions around the spherical framework(s) of  $C_{60}$  and of higher fullerenes in reactions which go well beyond simple mono- and bisaddition schemes. Accurate placement of functionalities on fullerenes with well-defined angle and distance relationships could provide useful tools for probing binding sites in biological systems through combinatorial methods.<sup>[43]</sup>

Since the nucleophilic step occurs first, as judged by the comparative rate studies shown in Scheme 6, initial addition of the *N,O*-ketene acetals **1a–e** occurs at a [6,6]-ring junction of  $C_{60}$  to give a partially delocalized anion in analogy to the formation of compound **10** (Scheme 17). Protonation of the intermediate fullereryl anion can give either the 1,2- (**3a–e**), 1,4- (**33a–e**), or 1,6-protonated intermediates (**34a–e**) before or after the tandem Diels–Alder reaction step (Scheme 2, Figure 16). Although 1,4- or even 1,6-protonation may occur

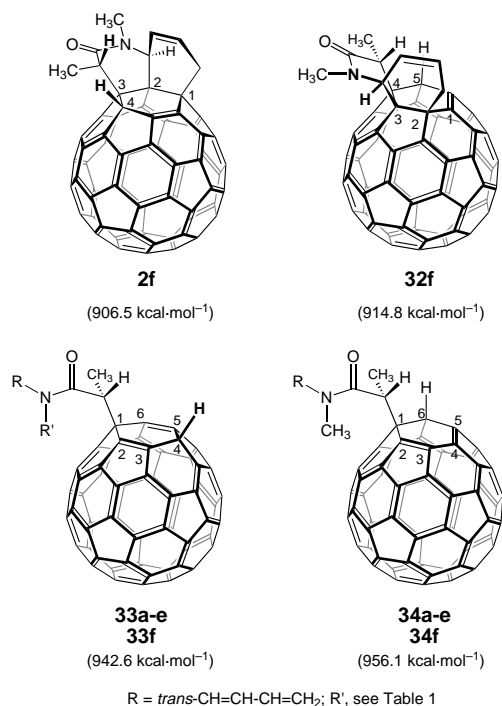


Figure 16. Structures of **2f**, its 2,3,4,5-regioisomer **32f**, and intermediates **33a–f** and **34a–34f**, the last leading to **32f**; corresponding AM1 calculated heats of formation ( $\text{kcal mol}^{-1}$ ) for the *N*-methylated systems.

to give intermediates **33a–e** or **34a–e** initially, followed by isomerization,<sup>[35a]</sup> this seems unlikely in the light of the fact that none of the corresponding products were seen in our experiments in the series **2a–e** or with product **10**. Additionally, the calculated heats of formation of the lowest energy conformers for model systems **33f** and **34f** are larger by 5.0 and 18.5  $\text{kcal mol}^{-1}$ , respectively, than that of **3f** (Figure 16).

The intramolecular Diels–Alder reaction of intermediates **3a–e** is constrained to only one of the two adjacent (*cis*-1) reaction centers as a corollary of the high diastereoselectivity of the reaction. The kinetic addition pathway saturating carbons C-3, C-4, and finally C-1, C-2 gives ample support for the 1,2,3,4-addition pattern of **2f**. Additionally, the 1,2,3,4-addition pattern of model system **2f** is calculated to have a lower heat of formation (8.3  $\text{kcal mol}^{-1}$ ) over the isomeric 2,3,4,5-product **32f** (Figure 16). This is reflected by the fact that **32f** incorporates a C=C double bond at a [5,6] ring junction, which is energetically unfavorable.<sup>[4]</sup> Provided that the tandem reaction were thermodynamically controlled (i.e. reversible), one would not expect the 2,3,4,5-product **32f** to be formed based upon these premises. Although 1,6-protonation to give intermediate **34f** rather than the 1,2-isomer **3f** (this could result from a suprafacial 1,5-shift similar to those of the diazomethane and azide additions),<sup>[4]</sup> ultimately resulting in the Diels–Alder product **32f**, cannot be entirely excluded, it is highly unlikely, since 6-protonation to give a [5,6] ring junction has never been observed and the energy of intermediate **34f** is very high.

**Stereoselectivity of the tandem nucleophilic/Diels–Alder additions:** The interesting *endo* stereoselectivity observed for the Diels–Alder step of the tandem reactions represents a somewhat counterintuitive outcome since it would appear that the *endo* products **2a–f**<sub>(endo)</sub> should be less favored than the *exo* products **2a–f**<sub>(exo)</sub> for steric reasons (Figure 17,

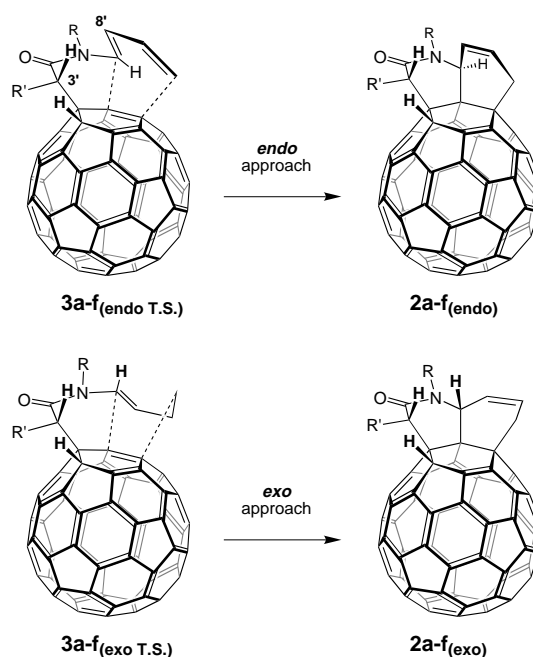


Figure 17. Product and transition-state structures for the *endo* and *exo* approaches in the Diels–Alder step of the tandem reactions.

Table 3). There is a significant 1,4-diaxial interaction in the transition states **3a-f**<sub>(endo)</sub> between H-3' of the installed propionamide moiety and C-8' of the approaching dienes. This interaction should be more demanding than the interaction arising between H-3' and H-8' in the *exo* transition states **3a-f**<sub>(exo)</sub>. The preferred *endo* selectivity in the Diels–Alder reaction is usually explained as a consequence of secondary orbital overlap interactions at the transition state forming between the dienophile and diene moieties.<sup>[44]</sup> Here, however, such effects would be negligible because of the inherent curvature of the  $\pi$  system in fullerenes, which points p orbitals away from the approaching diene p orbitals beyond the bond-forming centers as a result of the large pyramidalization angle into which the  $sp^2$  hybrids of  $C_{60}$  carbons are forced.<sup>[45]</sup>

The AM1 results for the *N*-isopropyl system **2a** confirm that the transition-state energies for **3a**<sub>(endo T.S.)</sub> and **3a**<sub>(exo T.S.)</sub> favor the former, but by only 0.5 kcal mol<sup>-1</sup> (Table 3). However, the *endo/exo* selectivity appears to be very sensitive to the size of the alkyl substituent on nitrogen, with a predicted reversal of selectivity for the *N*-methyl system **2f**, highlighting subtle steric effects from remote substituents on the transition-state energies. One should note that the conformational energies of these structures consistently favor those conformations in which the isopropyl group has the methine C–H bond *s-cis* to the amide N–C(=O) bond. These conformers are the ones observed in the 2D T-ROESY spectra, as revealed by the strong interactions displayed by both methyls with the axial hydrogen H<sub>c</sub> of the adjacent ring, but not by the *i*Pr methine proton H<sub>g</sub> with H<sub>e</sub> (see, for example, Figure 7).

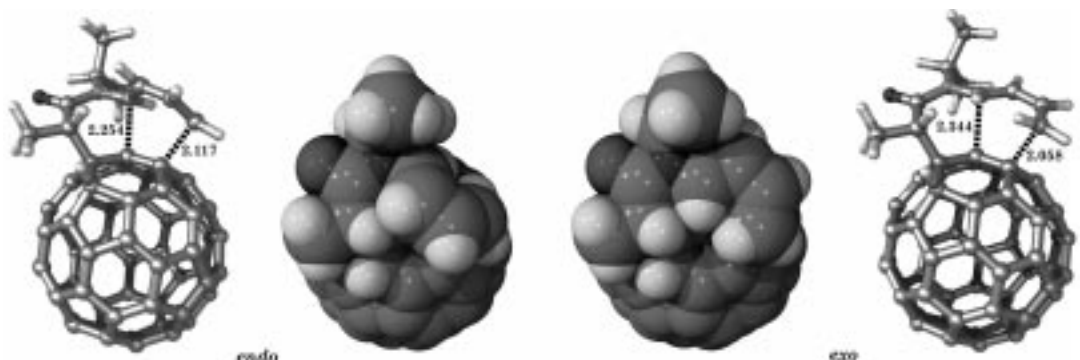
One of the issues to consider in these calculations is that the reaction barriers for the Diels–Alder step leading to **2a** or **2f** are too high at the AM1 level to account for the rates of the experimental reactions.<sup>[41]</sup> It is clear that the semiempirical level is unreliable in describing activation energies for these systems, even though AM1 calculated transition-state energies for acyclic Diels–Alder reactions tend to reproduce experimental activation energies better than low-level ab

initio calculations not incorporating electron correlation functionals.<sup>[46]</sup> Surprisingly, the AM1 barrier for the reaction of 1,3-butadiene with  $C_{60}$  is calculated to be 10 kcal mol<sup>-1</sup> lower ( $\Delta H^\ddagger = 16.2$  kcal mol<sup>-1</sup>) than for systems **3a** or **3f**, even though the latter are intramolecular.<sup>[42]</sup> Ab initio HF/STO-3G calculations, known to overestimate the Diels–Alder reaction barrier, give a value ( $\Delta H^\ddagger = 29.1$  kcal mol<sup>-1</sup>) that is roughly similar to those for **3a** or **3f**,<sup>[46, 47]</sup> but a direct comparison could not be made due to the computational limitations on these large systems in terms of locating transition states.

To increase the accuracy of calculation of energies, we have started a series of calculations to obtain single-point Becke3-LYP density functional energies based on ab initio 6-31G\* basis sets.<sup>[48]</sup> These results will be communicated separately in a more comprehensive computational study including additional experimental work to prepare the *N*-methylated system **2f**, as well as a consideration of polar silylated intermediates of type **29** in the transition states.

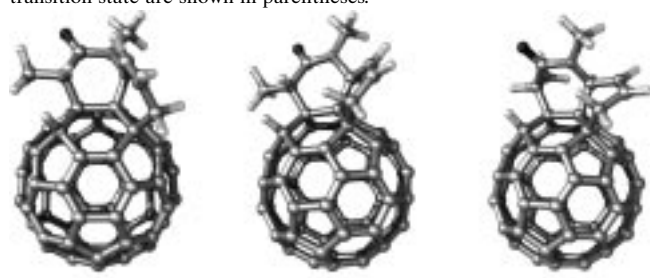
**Conformational preference of adducts 2a–e:** The conformational isomerism pointed out for adduct **2b** (Figure 4) is consistently in favor of the *endo* isomer (with respect to the alkene moiety) in adducts **2a–e**. Compound **2d'** is the exception (Table 5, below), but the *p*-methoxyphenyl substituent at C-3' has the opposite configuration to that in the methyl-, vinyl-, and *p*-methoxyphenyl-substituted compounds **2a–e**, while compound **2d'** is a product of an *exo* Diels–Alder addition and cannot undergo ring inversion. AM1 calculated energies for the two conformations of model compound **2f** give a clear preference for the *endo* conformer (4.8 kcal mol<sup>-1</sup>, corresponding to a  $\sim 3500:1$  ratio at 25 °C, Table 4). Furthermore, the calculated transition states are 12.7 and 17.5 kcal mol<sup>-1</sup> above the *exo* and *endo* conformers, respectively. These data indicate that the conformers should be able to exchange at the temperatures studied but that the very low preference for the *exo* conformer would make it undetectable by <sup>1</sup>H NMR.

Table 3. AM1-calculated transition-state structures **3a**<sub>(endo T.S.)</sub> and **3a**<sub>(exo T.S.)</sub> in wireframe and space-filling representations, energies (kcal mol<sup>-1</sup>) for the lowest energy conformers **3a** and **3f**, their respective *endo* and *exo s-cis* conformers closest to the transition-state geometries, the *endo* and *exo* transition states, and the *endo* and *exo* products (**2a** and **2f**) for the Diels–Alder step, with energy differences between them represented by  $\Delta E$ .



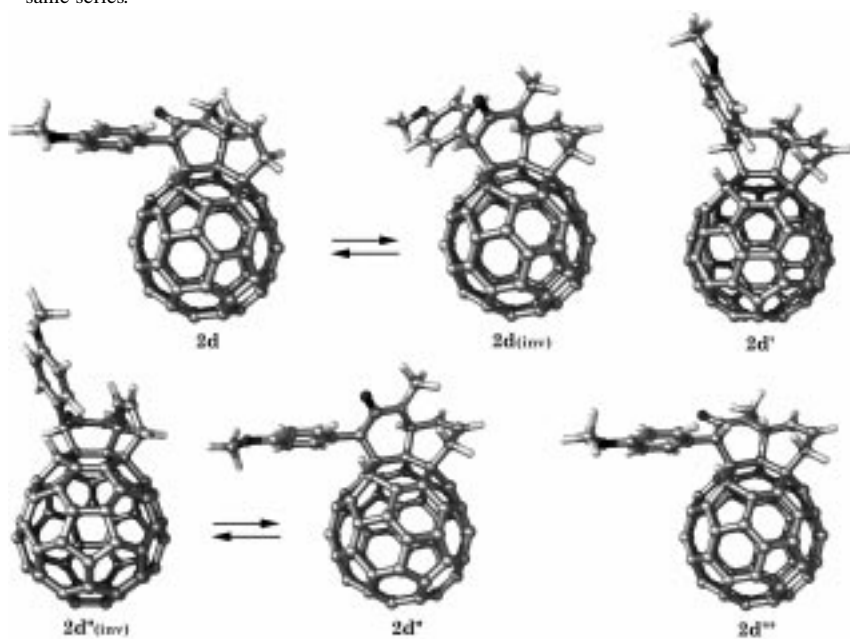
R	<b>3</b> (lowest conf.)	<b>3</b> ( <i>endo</i> conf.)	<b>3</b> ( <i>exo</i> conf.)	<b>3</b> ( <i>endo</i> T.S.)	$\Delta E$ ( <i>endo</i> – <i>exo</i> )	<b>3</b> ( <i>exo</i> T.S.)	<b>2</b> ( <i>endo</i> )	$\Delta E$ ( <i>endo</i> – <i>exo</i> )	<b>2</b> ( <i>exo</i> )
<i>i</i> Pr ( <b>a</b> )	930.0 (0) <sup>[b]</sup>	933.6 <sup>[a]</sup> (+3.6)	933.6 <sup>[b]</sup> (+3.6)	954.9 (+24.9)	(–0.5)	955.4 (+25.4)	897.7 (–32.3)	(–5.1)	902.8 (–27.2)
CH <sub>3</sub> ( <b>f</b> )	937.6 (0) <sup>[b]</sup>	942.7 (+5.1)	941.2 (+3.5)	963.9 (+26.3)	(+1.3)	962.6 (+25.0)	906.5 (–31.1)	(–4.8)	911.3 (–26.3)

Table 4. AM1-calculated structures and heats of formation ( $\text{kcal mol}^{-1}$ ) of the *endo* and *exo* conformations of **2f** and the transition state between them. Energy differences  $\Delta E$  between each of the two conformers and the transition state are shown in parentheses.



<i>endo</i>	T.S.	<i>exo</i>
<i>endo</i>	T.S.	<i>exo</i>
906.5 (-17.5)	924.0 (0)	911.3 (-12.7)

Table 5. AM1-calculated structures<sup>[a]</sup> and heats of formation ( $\text{kcal mol}^{-1}$ ) of the adducts **2d**–**d''**, of the unobserved isomer **2d'''**, and their complementary conformers. The *N*-(*p*-methoxy)benzyl substituent was replaced by a *N*-methyl substituent to simplify the conformational searches (MM3). Energy differences  $\Delta E$  are between products of the same series.



Conformer	<b>2d</b>	<b>2d'</b>	<b>2d''</b>	<b>2d'''</b>
observed	906.6 (0)	908.3 (+1.7)	911.2 (+4.6)	909.7 (+3.1)
ring-inverted (calculated)	912.7 (+6.1) <sup>[c]</sup>	– <sup>[b]</sup>	910.7 (-0.5) <sup>[c]</sup>	– <sup>[b]</sup>

[a] Only the lowest energy conformers, where rotation of the *p*-methoxyphenyl substituent gives more than one local minimum, are shown. [b] Only one bicyclic ring conformer exists for this compound. [c]  $\Delta E$  with complementary conformer.

**Conformational preference of the stereoisomeric adducts **2d**–**d''**:** The fact that all three diastereomers **2d**, **2d'**, and **2d''** are formed in the tandem reaction of **1d** with  $\text{C}_{60}$  may be a result of steric constraints in the Diels–Alder step in which intermediate **3d** undergoes intramolecular reaction from both *in* and *out* conformers in respect of the *p*-methoxyphenyl substituent, in addition to which the diene adds in an *endo* or

*exo* fashion (Table 5). The only product not formed is the one from the *out/exo* approach leading to compound **2d'''**, as this compound was not detected in the reaction mixtures. Additionally, the retro Michael-like isomerization of **2d''** to **2d'** observed at 75 °C indicates that equilibration may be another factor in the distribution of these products.

The low selectivity of this cycloaddition is rather puzzling, since products **2d'** and **2d''** result presumably from a transition state somewhat more strained than that for **3d** if they follow the same path as those of **3a**–**c** and **3e**. Compound **2d'** is the product of an *in* conformer adding in an *exo* fashion, while **2d''** is the complementary *endo* product as seen from the ring-inverted conformer **2d''(inv)** (conformers **2d(inv)** or **2d''** cannot form first because the starting diene geometry is *trans*). Both appear to require more strain in the transition state to place the *p*-methoxyphenyl ring above the reacting 6-membered ring, as suggested by the fact that the energy of the corresponding products (**2d'** and **2d''(inv)**) is higher than that of **2d**. One should note that compounds **2d'** and **2d'''** can only have one ring conformer as a result of the “*trans*” fusion of the bicyclic octahydroquinolinone system to the rigid core of  $\text{C}_{60}$ .

#### Formation of the 16-protonated and 16-alkylated derivatives:

The most useful aspect of the calculations performed in this study is their ability to explain (and predict) the sites of protonation and alkylation of anions generated from the tandem adducts **2a** and **2e**. The data assembled in Table 6 and Figure 18 support the experimental observations and greatly help in the assignment of alkylation positions.

The electronic structure of anion **17f** (Figure 18), representative of the experimental intermediates **17a** and **17e**, was expected to exert a large influence on the regiocontrol of electrophilic additions. The sites of highest charge densities, judged from a Mulliken population analysis (positions 4, 6, 14, 16, 21, and 35), contain a major part of the total anionic charge. This trend is reproduced in both representations showing HOMO coefficients and charge density projected on an electron potential surface (Figure 18). The sites of largest electron densities at positions 4 and 16 are those leading to the protonation and alkylation products **2f<sub>(4)</sub>** and **18f<sub>(16)</sub>** (Table 6), whereby steric requirements favor the 16-alkylated products against alkylation of the more reactive 4-position. Alkylation at C-6

does not happen because of the larger steric hindrance for approach at that site, reflected by the 4–8  $\text{kcal mol}^{-1}$  higher energies of the products **2f<sub>(6)</sub>** and **18f<sub>(6)</sub>**. The products of C-14 protonation or alkylation **2f<sub>(14)</sub>** and **18f<sub>(14)</sub>** are by far the most hindered, as seen by their much higher heats of formation. Calculations were carried out for the trimethylsilylated series **18g<sub>(4)</sub>**–**18g<sub>(35)</sub>** for their predictive power, and show that the

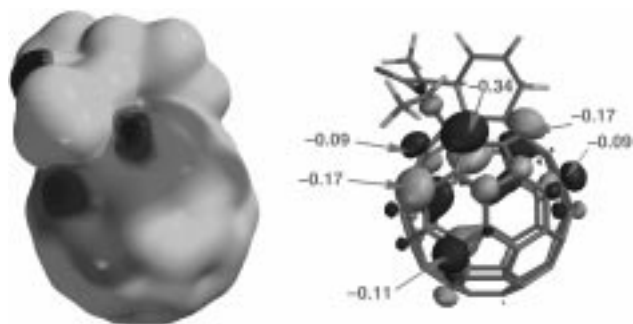


Figure 18. AM1 calculation results for anion **17f**: right: HOMO with electron density values for the corresponding carbons (Mulliken charges); left: anionic charge density projected on an electron potential surface ( $0.002 \text{ electron } \text{\AA}^{-2}$ ).

Table 6. AM1-calculated geometries and heats of formation ( $\text{kcal mol}^{-1}$ ) for compounds **2f**<sub>(4)</sub>–**2f**<sub>(35)</sub>, **18f**<sub>(4)</sub>–**18f**<sub>(35)</sub>, and trimethylsilylated systems **18g**<sub>(4)</sub>–**18g**<sub>(35)</sub>. Relative energies are given in parentheses, bold numbers are for those structures corresponding to the experimentally observed products.

R'	C-4	C-6	C-14	C-16	C-21	C-35
H	906.5 <b>(0)</b>	914.6 (+8.1)	925.3 (+18.8)	906.9 (+0.4)	919.0 (+12.5)	919.4 (+12.9)
Me	912.9 (0)	917.4 (+4.5)	935.3 (+22.4)	<b>(-6.2)</b>	916.7 (+3.8)	917.1 (+4.2)
SiMe <sub>3</sub>	885.6 (0)	888.1 (+2.5)	910.8 (+25.2)	872.3 (-13.3)	879.3 (-6.3)	879.4 (-6.2)

16-position is favored to a large extent, but that now the 21 and 35-positions are also favored. Although these experiments were not carried out for this study, use of a bulkier triisopropylsilyl or *tert*-butyldiphenylsilyl group would presumably result in silylation exclusively at the 35-position. Unusual 1,16-bis-silylated adducts were recently isolated upon reaction of bulky silyllithium anions with  $C_{60}$ ; their structures are related to the 1,2,3,35-isomer **18g**<sub>(35)</sub> by the relationship between the 3- and 35-positions.<sup>[49]</sup>

It should be noted that a double bond is located within a five-membered ring in both 6- and 16-alkylated products, which goes against the trend of most  $C_{60}$  adducts and is energetically unfavorable.<sup>[4]</sup> For the 1,2,3,35-alkylated products, there are two such unfavorable double bonds localized

in five-membered rings. The hydroxylated and alkylated products **18b**, **18c–e**, and **19** all have one double bond localized in a five-membered ring. Similarly, the kinetic product in the protonation of Fagan's *tert*-butyl  $C_{60}$  anion is 1,4-*t*Bu $C_{60}$ H, which slowly rearranges to 1,2-*t*Bu $C_{60}$ H with an activation energy of  $13.4 \text{ kcal mol}^{-1}$ .<sup>[28e, 35a]</sup> Hence, it is clear that steric hindrance can be made to play an active and important role in the control of functionalization of  $C_{60}$ . Conceivably, silylation products at the 35-position can be made to react with electrophilic reagents, an aspect of reactivity of fullerenes that has been little explored,<sup>[5a, 22, 50]</sup> or can serve as shielding groups in the addition of nucleophilic reagents. This will be tested in upcoming studies.

**Assignment of the methoxymethylation positions in compound 20:** The reaction of compound **19** with methoxide followed by methylation to give **20** posed the difficult problem of determining the exact locations of these two additions. The structural assignment of **20** was greatly facilitated by consideration of the most reactive electrophilic sites on the basis of the highest LUMO coefficients in the methoxide addition step, and the location of highest charge density in the ensuing methylation step. Correlation of these numbers with the experimental ROESY interactions (Figures 9 and 10) provides a convincing, albeit very indirect, answer to this structural problem.

Several interactions found in the 2D T-ROESY spectrum in the characterization section left only a few choices for the structure of product **20** if the nucleophilic addition and methylation steps proceed according to the criteria outlined above. The relative magnitudes of these interactions in most compounds were confirmed to be distance-dependent by the existence of very strong crosspeaks for distances of  $\sim 2.4 \text{ \AA}$ , for example Me<sub>(16)</sub> with H<sub>i</sub>, H<sub>i</sub> with H<sub>f</sub>, H<sub>f</sub> with H<sub>d</sub> in **20** according to the AM1-minimized geometry of the model system **20f** with an *N*-methyl group (Figures 9 and 18, right). The rigid conformation of the bicyclic octahydroquinolinone core in these structures does not allow these hydrogens to shift positions significantly on the NMR time scale with respect to the bicyclic conformational exchange discussed earlier. Thus, the „upper limit“ of observable interactions can be estimated at  $\sim 3.5 \text{ \AA}$  from a weak crosspeak between H<sub>f</sub> and H<sub>c</sub> in compound **20**, which is reproduced in the other compounds of similar conformation. Hence, crosspeak intensities were taken as a reliable indicator of distances to differentiate several structural candidates for compound **20**.

Considerations for the sites of attack by the methoxide anion are based on the fact that the magnitude of LUMO coefficients on monoadducts of  $C_{60}$  can be used to correlate the distribution of bisadducts of the bromomalonate anion addition in the Bingel reaction.<sup>[3, 12b]</sup> In precursor **19f** there are four sites with large LUMO coefficients at the 18-, 36-, 21-, and to a lesser extent 20-positions that are relevant to the structural assignments based on T-ROESY data (Figure 19). It is therefore not improbable that the methoxide anion reacts at only one of these sites as found by experiment. Addition of methoxide at C-36 can give anion **35a**, at the more hindered C-18 anion **35b**, at C-21 anion **35c**, and at C-20 anion **35d** (Figure 19). Each of these anions has only two or three sites of

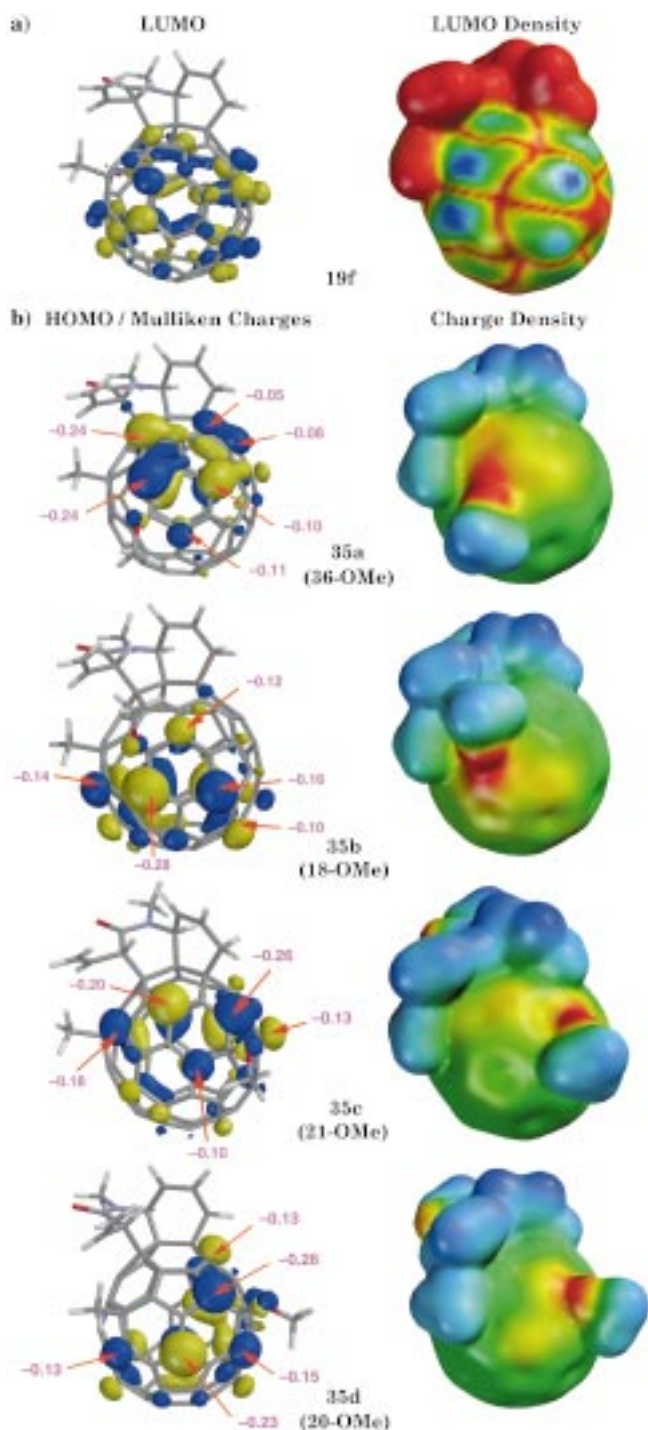


Figure 19. Calculated orbitals (AM1) for a) methylated adduct **19f** showing the LUMO and its projection on an electron potential surface ( $0.002 \text{ electron } \text{\AA}^{-2}$ ) and b) anions **35a-d** with their HOMOs, electron density values for corresponding carbons (Mulliken charges), and anionic charge densities projected on the corresponding electron potential surfaces ( $0.002 \text{ electron } \text{\AA}^{-2}$ ).

high HOMO orbital coefficients reproduced by electron-density values (Mulliken charges) and charge-density projections. Anion **35a** can react with methyl iodide at C-18, C-20, or C-4, but C-20 has a much weaker HOMO coefficient or charge density, and C-4 is strongly hindered sterically. Anion **35b** can react at C-36 or C-38, the first position being favored by electronics, and to a much lesser degree at C-34 and C-17.

Anion **35c** can react at C-5 or C-7, the latter being favored. Finally, anion **35d** can react at C-19 or C-36, the most likely position being C-19 according to the HOMO coefficients and charge densities.

The calculations and T-ROESY data are satisfied best by model structure **20(f)** (Figures 20 and 21). The weakest interactions in the 2D T-ROESY spectrum of **20** (Figure 10) are between  $\text{Me}_{(18)}$  and  $\text{H}_i$ ,  $\text{Me}_{(18)}$  and  $\text{Me}_{(16)}$ , and  $\text{Me}_{(18)}$  and  $\text{OMe}_{(36)}$ . Since the upper limit of observable interactions in these spectra is  $\sim 3.5 \text{ \AA}$ , structure **20(f)** is the only candidate having all its weakest correlating hydrogens within this range and its methoxylation–methylation positions within those dictated by the calculations. This assignment is in accord with the calculations in that addition of methoxide at C-36 should be favored by electronic and steric factors and the resulting anion **35a** should methylate at C-18.

Two other products (**20'** and **20''**) with their methoxy group at C-20 and their second methyl group at C-19 and C-36, respectively, were also considered based on the geometrical restrictions deduced from the 2D T-ROESY data, but the

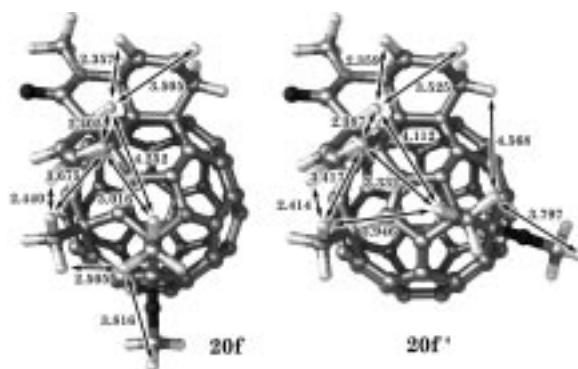


Figure 20. AM1 calculated geometries of model compounds **20f** and **20f'** with relevant atomic distances.

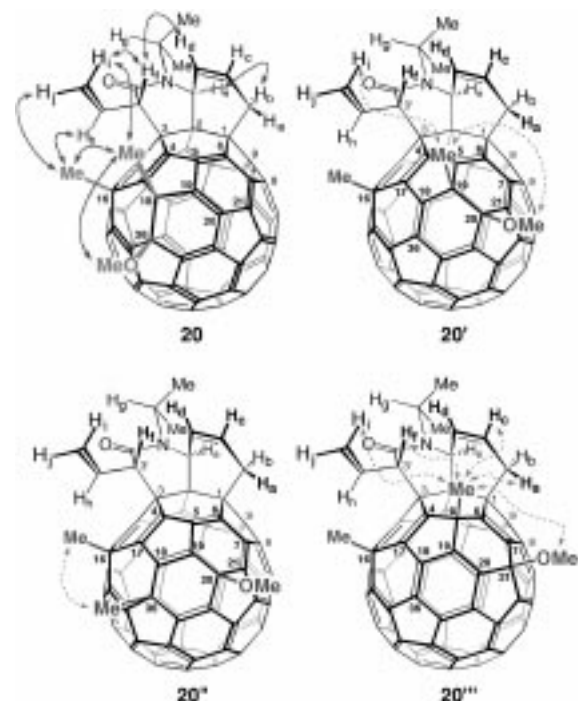
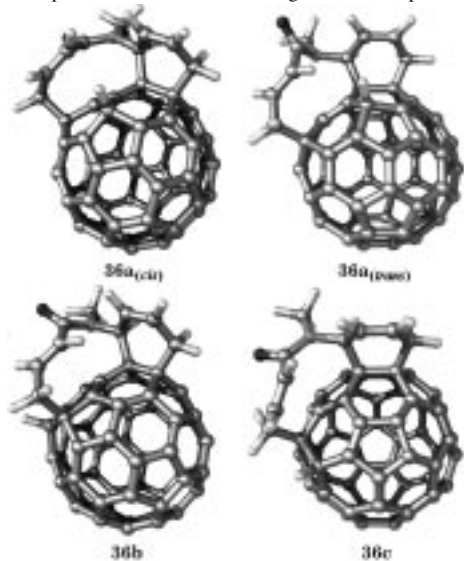


Figure 21. Structures **20**, **20'**, **20''**, and **20'''** and their observed or likely diagnostic proton–proton interactions.

Table 7. AM1-calculated structures and heats of formation (kcal mol<sup>-1</sup>) of the potential Cope rearrangement products **36a–c** and **37a–c**. The energies of the precursors **2h** and **19h** are given for comparison.



R	<b>2h</b> <sub>(4)</sub>	<b>36a</b> <sub>(cis)</sub>	<b>36a</b> <sub>(trans)</sub>	<b>2h</b> <sub>(16)</sub>	<b>36b</b>	<b>36c</b>
H	932.1 (0)	933.4 (+1.7)	935.9 (+3.8)	933.4 (0)	941.7 (+8.3)	948.3 (+14.9)
	<b>19h</b> <sub>(4)</sub>	<b>37a</b> <sub>(cis)</sub>	<b>37a</b> <sub>(trans)</sub>	<b>19h</b> <sub>(16)</sub>	<b>37b</b>	<b>37c</b>
CH <sub>3</sub>	938.9 (0)	933.5 (-5.4)	935.4 (-3.5)	932.6 (0)	946.4 (+13.8)	951.2 (+18.6)

calculated lower coefficient of the LUMO orbital at C-20 of model precursor **19f**, where the methoxy group would have to add first for both products, makes them much less likely to form. Furthermore, the distance for **20'** between the closest protons of Me<sub>(19)</sub> and Me<sub>(16)</sub> in their AM1 minimized geometry is 3.946 Å, and that of Me<sub>(19)</sub> and H<sub>i</sub> is 3.332 Å. The interaction observed between Me<sub>(16)</sub> and Me<sub>(18)</sub> in **20** would therefore not be seen between Me<sub>(16)</sub> and Me<sub>(19)</sub> in **20'**. For **20''**, there would be no interaction between H<sub>i</sub> and Me<sub>(36)</sub>, which is present in **20** (H<sub>i</sub> and Me<sub>(18)</sub>). This also why the methylation product derived from anion **35b** was not considered.

A last alternative structure (**20'''**) that would be in part in accord with the 2D T-ROESY data was also considered (Figure 21). Placing the methyl group at the 5-position (and the methoxy at the 21-position) is a possible alternative because it is compatible with the calculations showing the presence of a substantial LUMO coefficient at C-21 of **19** where methoxide could have attacked (Figure 19). The resulting anion is localized at both C-7 and C-5 and could give the kinetic methylation product **20'''**. However, this structure can be rejected on the basis of the interaction existing between Me<sub>(18)</sub> and Me<sub>(16)</sub> in **20**. The interaction of Me<sub>(5)</sub> with Me<sub>(16)</sub> in **20'''** should be nonexistent since the distance between the closest protons of Me<sub>(5)</sub> and Me<sub>(16)</sub> is 4.152 Å. Moreover, there should be additional strong interactions between Me<sub>(5)</sub> and H<sub>i</sub>, H<sub>a</sub>, and H<sub>c</sub> that are not observed in the spectrum of Figure 10.

**Potential Cope rearrangement products:** The inability of the vinylic compounds **2e** and **19** to undergo a Cope rearrange-

ment despite their high thermal stability was examined theoretically (Scheme 13, Table 7). Not surprisingly, it was found that none of the systems corresponding to the expected experimental products (**36a** for **24**, **37b** and **37c** for **19**) is lower in energy than the starting materials **2h**<sub>(4)</sub> and **19h**<sub>(16)</sub>, and therefore they should not undergo the rearrangement. The least unfavorable model system equivalent to the Cope rearrangement of **2e** to **24** (**2h**<sub>(4)</sub> to **36a**) is endothermic by 1.7 kcal mol<sup>-1</sup>. However, the rearrangement of the analogous 4-methylated product **19h**<sub>(4)</sub> to **37a** is favored by 5.4 kcal mol<sup>-1</sup>, but this methylation product was not obtained in the alkylation experiments. Both systems **2h**<sub>(4)</sub> and **19h**<sub>(4)</sub> can undergo a Cope rearrangement via a chair transition state to give a *cis*-olefin or a boat transition state to give a *trans*-olefin. The *trans* configuration is determined by the starting low-energy conformation, but boat transition states are generally higher than chairs in 3,3-sigmatropic rearrangements and the corresponding products **36a**<sub>(trans)</sub> or **37a**<sub>(trans)</sub> are higher in energy than their *cis* counterparts.<sup>[46, 51]</sup> Both *trans* products also have strongly distorted amide bonds.

The results of the calculations for the systems **36a**<sub>(cis)</sub> or **37a**<sub>(cis)</sub> indicate that there is potential in exploring other Cope systems on fullerenes, especially if some additional energetic incentive within the allylic moiety in the departing structure can be added (anchoring through a quarternary center, oxyanion to enolate conversion, etc.). These and other prospects of further functionalization around the spherical surface of C<sub>60</sub> will be investigated in forthcoming work.

## Conclusion

The enhanced reactivity of the *N,O*-ketene *N*-1,3-butadienyl-*N*-alkyl-*O*-silyl acetals **1a–e** with C<sub>60</sub> allows the formation of the sterically congested adducts **2a–e** with high diastereoselectivity proceeding through a tandem process. Alkylation of the anions resulting from deprotonation of the fulleranyl hydrogen at C-4 introduces a supplementary handle on the fullerene at C-16 from which there are potentially a number of higher adducts that can be formed with high regioselectivity, as shown by the formation of the methoxydimethylated product **20**. Structural characterization of all these products is greatly facilitated by the use of standard 2D NMR techniques and does not necessarily require C–C correlations from expensive <sup>13</sup>C-labeled fullerenes to give satisfactory structural characterization. Calculated energies and electronic structures of the compounds were found to corroborate the experimental findings and in some cases were used as guides for the characterization of the structures.

Tandem reactions leading to constrained systems, such as the 1,2,3,4-tetrahydrofullerenes described in this study, have the potential to lead to a host of highly functionalized structures that resemble biologically active products because their reduced fullerene π surface lowers their electrophilic and electron-accepting properties, and functional groups can be brought in to increase hydrophilicity. The potential of combinatorial synthesis, which can be easily implemented with these systems, is very high and is currently being examined in our laboratories. It will be interesting in this regard to determine if the relatively low yields in several of

the reactions described in this work can be increased by supporting the substrates on polymer beads. The issue of nonquantitative yielding reactions in fullerene chemistry is one that has consistently lowered efforts to promote multistep syntheses and that has not been explained. Although regioisomers can form from reactions at the many double bonds,<sup>[4]</sup> it is usually polymeric material which appears to contribute to the lower overall yields of reactions. We suspect that single electron transfer side reactions promote radical polymerization of the fullerene units to give rapidly insoluble oligomeric by-products. These aspects should be resolved by polymer-supported reactions.

## Experimental Section

A full account of the experimental conditions, characterization data, and <sup>1</sup>H NMR spectra of compounds **2d'**/**2d''** (2-DT-ROESY) are provided in the Supporting Information.

## Acknowledgments

We thank Dr. Jane Strouse at UCLA for assistance with the 2D NMR experiments, and Prof. Ken Houk for helpful discussions on computational results. This work was supported in part by an NSF Young Investigator Award (CHE-9457693) (Y.R.), an Arnold and Mabel Beckman Young Investigator Award (Y.R.), and by the Swiss National Foundation (R.N.). The generous support of the Swiss National Science Foundation for a postdoctoral fellowship (A.F.) is also greatly appreciated.

- [1] M. J. Arce, A. L. Viado, Y. Z. An, S. I. Khan, Y. Rubin, *J. Am. Chem. Soc.* **1996**, *118*, 3775–3776.
- [2] a) Y. Rubin, *Chem. Eur. J.* **1997**, *3*, 1009–1016; b) Y. Rubin, *Chimia* **1998**, *52*, 118–126; c) Y. Rubin, *Top. Curr. Chem.* **1999**, *199*, 67–91; d) G. Schick, T. Jarrosson, Y. Rubin, *Angew. Chem.* **1999**, *111*, 2508–2512; *Angew. Chem. Int. Ed.* **1999**, *38*, 2360–2363.
- [3] F. Djojo, A. Herzog, I. Lamparth, F. Hampel, A. Hirsch, *Chem. Eur. J.* **1996**, *2*, 1537–1547.
- [4] a) A. Hirsch, *The Chemistry of the Fullerenes*, Thieme, New York, **1994**; b) F. Diederich, C. Thilgen, *Science* **1996**, *271*, 317–323; c) A. Hirsch, *Top. Curr. Chem.* **1999**, *199*, 1–65.
- [5] a) A. G. Avent, P. R. Birkett, J. D. Crane, A. D. Darwish, G. J. Langley, H. W. Kroto, R. Taylor, D. R. M. Walton, *J. Chem. Soc. Chem. Commun.* **1994**, 1463–1464; b) P. R. Birkett, A. G. Avent, A. D. Darwish, H. W. Kroto, R. Taylor, D. R. M. Walton, *J. Chem. Soc. Chem. Commun.* **1993**, 1230–1232; c) P. R. Birkett, P. B. Hitchcock, H. W. Kroto, R. Taylor, D. R. M. Walton, *Nature* **1992**, *357*, 479–481; d) F. N. Tebbe, R. L. Harlow, D. B. Chase, D. L. Thorn, G. C. Campbell, Jr., J. C. Calabrese, N. Herron, R. J. Young, Jr., E. Wasserman, *Science* **1992**, *256*, 822–825.
- [6] a) Q. Lu, D. I. Schuster, S. R. Wilson, *J. Org. Chem.* **1996**, *61*, 4764–4768; b) R. J. Cross, H. A. Jimenez-Vazquez, Q. Lu, M. Saunders, D. I. Schuster, S. R. Wilson, H. Zhao, *J. Am. Chem. Soc.* **1996**, *118*, 11454–11459; c) S. R. Wilson, Q. Lu, *Tetrahedron Lett.* **1995**, *36*, 5707–5710.
- [7] a) L. Pasimeni, A. Hirsch, I. Lamparth, A. Herzog, M. Maggini, M. Prato, C. Corvaja, G. Scorrano, *J. Am. Chem. Soc.* **1997**, *119*, 12896–12901; b) L. Pasimeni, A. Hirsch, I. Lamparth, M. Maggini, M. Prato, *J. Am. Chem. Soc.* **1997**, *119*, 12902–12905.
- [8] a) R. Schwenninger, T. Müller, B. Kräutler, *J. Am. Chem. Soc.* **1997**, *119*, 9317–9318; b) B. Kräutler, J. Maynollo, *Tetrahedron* **1996**, *52*, 5033–5042; c) B. Kräutler, T. Müller, J. Maynollo, K. Gruber, C. Kratky, P. Ochsenbein, D. Schwarzenbach, H. B. Bürgi, *Angew. Chem.* **1996**, *108*, 1294–1296; *Angew. Chem. Int. Ed. Engl.* **1996**, *35*, 1204–1206; d) B. Kräutler, J. Maynollo, *Angew. Chem.* **1995**, *107*, 69–71; *Angew. Chem. Int. Ed. Engl.* **1995**, *34*, 87–88.
- [9] a) F. Diederich, R. Kessinger, *Acc. Chem. Res.* **1999**, *32*, 537–545; b) J. P. Bourgeois, L. Echevoyen, M. Fibbioli, E. Pretsch, F. Diederich, *Angew. Chem.* **1998**, *110*, 2203–2207; *Angew. Chem. Int. Ed.* **1998**, *37*, 2118–2121; c) J. F. Nierengarten, T. Habicher, R. Kessinger, F. Cardullo, F. Diederich, V. Gramlich, J. P. Gisselbrecht, C. Boudon, M. Gross, *Helv. Chim. Acta* **1997**, *80*, 2238–2276; d) L. Isaacs, F. Diederich, R. F. Haldimann, *Helv. Chim. Acta* **1997**, *80*, 317–342; e) F. Cardullo, L. Isaacs, F. Diederich, J. P. Gisselbrecht, C. Boudon, M. Gross, *Chem. Commun.* **1996**, 797–799; f) L. Isaacs, P. Seiler, F. Diederich, *Angew. Chem.* **1995**, *107*, 1636–1639; *Angew. Chem. Int. Ed. Engl.* **1995**, *34*, 1466–1469; g) C. Boudon, J. P. Gisselbrecht, M. Gross, L. Isaacs, H. L. Anderson, R. Faust, F. Diederich, *Helv. Chim. Acta* **1995**, *78*, 1334–1344; h) L. Isaacs, R. F. Haldimann, F. Diederich, *Angew. Chem.* **1994**, *106*, 2434–2437; *Angew. Chem. Int. Ed. Engl.* **1994**, *33*, 2339–2342.
- [10] a) P. P. Kanakamma, S. L. Huang, C. G. Juo, G. R. Her, T. Y. Luh, *Chem. Eur. J.* **1998**, *4*, 2037–2042; b) C. K. F. Shen, H. Yu, C.-G. Juo, K.-M. Chien, G.-R. Her, T.-Y. Luh, *Chem. Eur. J.* **1997**, *3*, 744–748; c) C. K. F. Shen, K. M. Chien, C. G. Juo, G. R. Her, T. Y. Luh, *J. Org. Chem.* **1996**, *61*, 9242–9244; d) L. L. Shiu, K. M. Chien, T. Y. Liu, T. I. Lin, G. R. Her, T. Y. Luh, *J. Chem. Soc. Chem. Commun.* **1995**, 1159–1160; e) G. X. Dong, J. S. Li, T. H. Chan, *J. Chem. Soc. Chem. Commun.* **1995**, 1725–1726.
- [11] a) H. Isobe, H. Tokuyama, M. Sawamura, E. Nakamura, *J. Org. Chem.* **1997**, *62*, 5034–5041; b) M. Taki, S. Sugita, Y. Nakamura, E. Kasashima, E. Yashima, Y. Okamoto, J. Nishimura, *J. Am. Chem. Soc.* **1997**, *119*, 926–932; c) E. Nakamura, H. Isobe, H. Tokuyama, M. Sawamura, *Chem. Commun.* **1996**, 1747–1748.
- [12] a) A. W. Jensen, A. Khong, M. Saunders, S. R. Wilson, D. I. Schuster, *J. Am. Chem. Soc.* **1997**, *119*, 7303–7307; b) I. Lamparth, B. Nuber, G. Schick, A. Skiebe, T. Grösser, A. Hirsch, *Angew. Chem.* **1995**, *107*, 2473–2476; *Angew. Chem. Int. Ed. Engl.* **1995**, *34*, 2257–2259; c) A. L. Balch, D. A. Costa, B. C. Noll, M. M. Olmstead, *J. Am. Chem. Soc.* **1995**, *117*, 8926–8932; d) C. C. Henderson, C. M. Rohlffing, R. A. Assink, P. A. Cahill, *Angew. Chem.* **1994**, *106*, 803–808; *Angew. Chem. Int. Ed. Engl.* **1994**, *33*, 786–788; e) M. S. Meier, F. S. Corbin, V. K. Vance, M. Clayton, M. Mollman, *Tetrahedron Lett.* **1994**, *35*, 5789–5792; f) H. Takeshita, J. F. Liu, N. Kato, A. Mori, *Tetrahedron Lett.* **1994**, *35*, 6305–6308.
- [13] S. H. Friedman, G. L. Kenyon, *J. Am. Chem. Soc.* **1997**, *119*, 447–448.
- [14] a) S. E. Denmark, A. Thorarensen, *Chem. Rev.* **1996**, *96*, 137–166; b) J. D. Winkler, *Chem. Rev.* **1996**, *96*, 167–176; c) I. Ryu, N. Sonoda, D. P. Curran, *Chem. Rev.* **1996**, *96*, 177–194; d) P. J. Parsons, C. S. Penkett, A. J. Shell, *Chem. Rev.* **1996**, *96*, 195–206; e) L. F. Tietze, U. Beifuss, *Angew. Chem.* **1993**, *105*, 137–170; *Angew. Chem. Int. Ed. Engl.* **1993**, *32*, 131–163; f) K. Neuschütz, J. Velker, R. Neier, *Synthesis* **1998**, 227–255.
- [15] For the reaction of analogous *O,O*-ketene-*O*-alkyl-*O*-silyl acetals, see: a) K. Mikami, S. Matsumoto, A. Ishida, S. Takamuku, T. Suenobu, S. Fukuzumi, *J. Am. Chem. Soc.* **1995**, *117*, 11134–11141; b) K. Mikami, S. Matsumoto, *Synlett* **1995**, 229–230; c) H. Tokuyama, H. Isobe, E. Nakamura, *J. Chem. Soc. Chem. Commun.* **1994**, 2753–2754.
- [16] a) A. Franz, P. Y. Eschler, M. Tharin, H. Stoeckli-Evans, R. Neier, *Synthesis* **1996**, 1239–1245; b) A. Franz, P. Y. Eschler, M. Tharin, R. Neier, *Tetrahedron* **1996**, *52*, 11643–11656; c) M. Baak, Y. Rubin, A. Franz, H. Stoeckli-Evans, L. Bigler, J. Nachbauer, R. Neier, *Chimia* **1993**, *47*, 233–240; d) W. Oppolzer, L. Bieber, E. Francotte, *Tetrahedron Lett.* **1979**, 981–984.
- [17] a) S. R. Wilson, Q. Y. Lu, J. R. Cao, Y. H. Wu, C. J. Welch, D. I. Schuster, *Tetrahedron* **1996**, *52*, 5131–5142; b) S. R. Wilson, Q. Y. Lu, *Tetrahedron Lett.* **1993**, *34*, 8043–8046.
- [18] a) Y. Z. An, G. A. Ellis, A. L. Viado, Y. Rubin, *J. Org. Chem.* **1995**, *60*, 6353–6361; b) J. M. Lawson, A. M. Oliver, D. F. Rothenfluh, Y. Z. An, G. A. Ellis, M. G. Ranasinghe, S. I. Khan, A. G. Franz, P. S. Ganapathi, M. J. Shephard, M. N. Paddon-Row, Y. Rubin, *J. Org. Chem.* **1996**, *61*, 5032–5054; c) M. J. Arce, A. L. Viado, S. I. Khan, Y. Rubin, *Organometallics* **1996**, *15*, 4340–4342; d) Y. Z. An, A. L. Viado, M. J. Arce, Y. Rubin, *J. Org. Chem.* **1995**, *60*, 8330–8331.
- [19] X. J. Zhang, A. Romero, C. S. Foote, *J. Am. Chem. Soc.* **1993**, *115*, 11024–11025.
- [20] S. Hünig, H. Kahanek, *Chem. Ber.* **1957**, *90*, 238–245. For the lack of Diels–Alder products with the isomeric 2-dialkylaminobutadienes, see: M. L. Farmer, W. E. Billups, R. B. Greenlee, A. N. Kurtz, *J. Org. Chem.* **1966**, *31*, 2885–2887.

- [21] a) J. Schoepfer, C. Marquis, C. Pasquier, R. Neier, *J. Chem. Soc. Chem. Commun.* **1994**, 1001–1002; b) T. Matsui, Y. Matsushita, M. Nakayama, *Heterocycles* **1992**, *34*, 723–728; c) E. C. Gravett, J. A. K. Howard, K. Mackenzie, S.-X. Liu, P. B. Karadakov, *J. Chem. Soc. Chem. Commun.* **1991**, 1763–1765; d) F. Backenstrass, J. Streith, T. Tschamber, *Tetrahedron Lett.* **1990**, *31*, 2139–2142; e) R. Gleiter, M. Karcher, *Angew. Chem.* **1988**, *100*, 851–852; *Angew. Chem. Int. Ed. Engl.* **1988**, *27*, 840–841; f) T. Matsui, S. Kitajima, M. Nakayama, *Bull. Chem. Soc. Jpn.* **1988**, *61*, 316–318; g) S. Huber, P. Stamouli, T. Jenny, R. Neier, *Helv. Chim. Acta* **1986**, *69*, 1898–1915.
- [22] For the first report on a hydroxylated fullerene, see: P. R. Birkett, A. G. Avent, A. D. Darwish, H. W. Kroto, R. Taylor, D. R. M. Walton, *Chem. Commun.* **1996**, 1231–1232.
- [23] For a similar hydroxylation in the synthesis of Taxol, see: P. A. Wender, N. F. Badham, S. P. Conway, P. E. Floreancig, T. E. Glass, C. Gränicher, J. B. Houze, J. Jänichen, D. S. Lee, D. G. Marquess, P. L. McGrane, W. Meng, T. P. Mucciario, M. Mühlebach, M. G. Natchus, H. Paulsen, D. B. Rawlins, J. Satkofsky, A. J. Shuker, J. C. Sutton, R. E. Taylor, K. Tomooka, *J. Am. Chem. Soc.* **1997**, *119*, 2755–2756.
- [24] C. Bingel, *Chem. Ber.* **1993**, *126*, 1957–1959.
- [25] a) J. S. Chen, K. N. Houk, C. S. Foote, *J. Am. Chem. Soc.* **1997**, *119*, 9852–9855; b) T. H. W. Poon, S. H. Park, Y. Elemes, C. S. Foote, *J. Am. Chem. Soc.* **1995**, *117*, 10468–10473.
- [26] a) J. M. Hawkins, S. Loren, A. Meyer, R. Nunlist, *J. Am. Chem. Soc.* **1991**, *113*, 7770–7771; b) J. M. Hawkins, A. Meyer, T. A. Lewis, U. Bunz, R. Nunlist, G. E. Ball, T. W. Ebbesen, K. Tanigaki, *J. Am. Chem. Soc.* **1992**, *114*, 7954–7955.
- [27] For the spectral analysis of complex coupling patterns, see, for example: a) J. B. Lambert, H. F. Shurvell, D. A. Lightner, R. G. Cooks, in *Organic Structural Spectroscopy*, Prentice-Hall, Upper Saddle River (NJ 07458), **1998**, pp. 75–79.
- [28] a) R. G. Bergosh, M. S. Meier, J. A. L. Cooke, H. P. Spielmann, B. R. Weedon, *J. Org. Chem.* **1997**, *62*, 7667–7672; b) L. B. Alemany, A. Gonzalez, W. E. Billups, M. R. Willcott, E. Ezell, E. Gozansky, *J. Org. Chem.* **1997**, *62*, 5771–5779; c) P. Timmerman, H. L. Anderson, R. Faust, J. F. Nierengarten, T. Habicher, P. Seiler, F. Diederich, *Tetrahedron* **1996**, *52*, 4925–4947; d) M. E. Niyazymbetov, D. H. Evans, S. A. Lerke, P. A. Cahill, C. C. Henderson, *J. Phys. Chem.* **1994**, *98*, 13093–13098; e) P. J. Fagan, P. J. Krusic, D. H. Evans, S. A. Lerke, E. Johnston, *J. Am. Chem. Soc.* **1992**, *114*, 9697–9699.
- [29] Y. Murata, K. Motoyama, K. Komatsu, T. S. M. Wan, *Tetrahedron* **1996**, *52*, 5077–5090.
- [30] P. S. Ganapathi, S. H. Friedman, G. L. Kenyon, Y. Rubin, *J. Org. Chem.* **1995**, *60*, 2954–2955.
- [31] T.-S. Hwang, A. J. Shaka, *J. Am. Chem. Soc.* **1992**, *114*, 3157–3159.
- [32] a) S. Fukuzumi, T. Suenobu, T. Hirasaka, R. Arakawa, K. M. Kadish, *J. Am. Chem. Soc.* **1998**, *120*, 9220–9227; b) Y. Murata, M. Shiro, K. Komatsu, *J. Am. Chem. Soc.* **1997**, *119*, 8117–8118; c) H. Okamura, Y. Murata, M. Minoda, K. Komatsu, T. Miyamoto, T. S. M. Wan, *J. Org. Chem.* **1996**, *61*, 8500–8502; d) Y. Murata, K. Komatsu, T. S. M. Wan, *Tetrahedron Lett.* **1996**, *37*, 7061–7064; e) A. Hirsch, T. Grösser, A. Skieba, A. Soi, *Chem. Ber.* **1993**, *126*, 1061–1067; f) A. Hirsch, A. Soi, H. R. Karfunkel, *Angew. Chem.* **1992**, *104*, 808–810; *Angew. Chem. Int. Ed. Engl.* **1992**, *31*, 766–768.
- [33] a) R. Borghi, L. Lunazzi, G. Placucci, P. J. Krusic, D. A. Dixon, N. Matsuzawa, M. Ata, *J. Am. Chem. Soc.* **1996**, *118*, 7608–7617; b) J. R. Morton, K. F. Preston, P. J. Krusic, S. A. Hill, E. Wasserman, *J. Am. Chem. Soc.* **1992**, *114*, 5454–5455; c) J. R. Morton, K. F. Preston, P. J. Krusic, S. A. Hill, E. Wasserman, *J. Phys. Chem.* **1992**, *96*, 3576–3578; d) P. J. Krusic, E. Wasserman, P. N. Keizer, J. R. Morton, K. F. Preston, *Science* **1991**, *254*, 1183–1185.
- [34] A. Franz, Y.-Z. An, P. S. Ganapathi, R. Neier, Y. Rubin, in *Fullerenes Proceedings Series: Recent Advances in the Chemistry and Physics of Fullerenes and Related Materials, Vol. 3* (Eds.: K. M. Kadish, R. S. Ruoff), Electrochemical Society, Pennington, New Jersey, **1996**, pp. 1326–1341.
- [35] a) F. Banim, D. J. Cardin, P. Heath, *Chem. Commun.* **1997**, 25–26.; b) S. Ballenweg, R. Gleiter, W. Krätschmer, *Tetrahedron Lett.* **1993**, *34*, 3737–3740.
- [36] Vicinal coupling constants for H-C<sub>(sp<sup>3</sup>)</sub>-C<sub>(sp<sup>3</sup>)</sub>-H pathways follow an angle dependence similar to the Karplus correlation curve for H-C<sub>(sp<sup>3</sup>)</sub>-C<sub>(sp<sup>3</sup>)</sub>-H dihedral angles: A. A. Bothner-By, *Adv. Magn. Reson.* **1965**, *1*, 195–316.
- [37] a) S. R. Wilson, Y. H. Wu, *J. Am. Chem. Soc.* **1993**, *115*, 10334–10337; b) G. W. Wang, L. H. Shu, S. H. Wu, H. M. Wu, X. F. Lao, *J. Chem. Soc. Chem. Commun.* **1995**, 1071–1072.
- [38] For a report on SET being involved in the Diels–Alder reaction of electron-rich dienes with C<sub>60</sub>, see: K. Mikami, S. Matsumoto, Y. Okubo, T. Suenobu, S. Fukuzumi, *Synlett*, **1999**, 1130–1133.
- [39] For other reactions resulting from initial photoinduced electron transfer with triplet excited C<sub>60</sub>, see: a) K. Mikami, S. Matsumoto, T. Tono, T. Suenobu, A. Ishida, S. Fukuzumi, *Synlett* **1997**, 85–87; b) W. Zhang, Y. Su, L. B. Gan, J. F. Jiang, C. H. Huang, *Chem. Lett.* **1997**, 1007–1008; c) S. H. Wu, D. W. Zhang, G. W. Wang, L. H. Shu, H. M. Wu, J. F. Xu, X. F. Lao, *Synth. Commun.* **1997**, *27*, 2289–2298; d) C. Siedschlag, H. Luftmann, C. Wolff, J. Mattay, *Tetrahedron* **1997**, *53*, 3587–3592; e) K. F. Liou, C. H. Cheng, *Chem. Commun.* **1996**, 1423–1424; f) G. Lem, D. I. Schuster, S. H. Courtney, Q. Y. Lu, S. R. Wilson, *J. Am. Chem. Soc.* **1995**, *117*, 554–555; g) G. E. Lawson, A. Kitaygorodskiy, B. Ma, C. E. Bunker, Y. P. Sun, *J. Chem. Soc. Chem. Commun.* **1995**, 2225–2226; h) M. R. Banks, J. I. G. Cadogan, I. Gosney, P. K. G. Hodgson, P. R. R. Langridge-Smith, J. R. A. Millar, J. A. Parkinson, I. H. Sadler, A. T. Taylor, *J. Chem. Soc. Chem. Commun.* **1995**, 1171–1172; i) J. Averdung, E. Albrecht, J. Lauterwein, H. Luftmann, J. Mattay, H. Mohn, W. H. Müller, H. U. ter Meer, *Chem. Ber.* **1994**, *127*, 787–789; j) S. R. Wilson, N. Kaprinidis, Y. H. Wu, D. I. Schuster, *J. Am. Chem. Soc.* **1993**, *115*, 8495–8496; k) D. I. Schuster, J. R. Cao, N. Kaprinidis, Y. H. Wu, A. W. Jensen, Q. Y. Lu, H. Wang, S. R. Wilson, *J. Am. Chem. Soc.* **1996**, *118*, 5639–5647.
- [40] For a correlation of Diels–Alder reactivity and photoelectron ionization potentials of dienamides similar to **13**, see: L. E. Overman, G. F. Taylor, K. N. Houk, I. N. Domelsmith, *J. Am. Chem. Soc.* **1978**, *100*, 3182–3189.
- [41] For activation energies of cyclopentadiene and 9,10-dimethylanthracene Diels–Alder reactions, see: J. Sauer, H. Wiest, A. Milert, *Chem. Ber.* **1964**, *97*, 3183–3207.
- [42] For reviews on the intramolecular Diels–Alder reaction and theoretical aspects, see: a) W. Oppolzer, *Angew. Chem.* **1977**, *89*, 10–24; *Angew. Chem. Int. Ed. Engl.* **1977**, *16*, 10–23; b) G. Brieger, J. N. Bennett, *Chem. Rev.* **1980**, *80*, 63–97; A. G. Fallis, *Can. J. Chem.* **1984**, *62*, 183–234; d) D. Craig, *Chem. Soc. Rev.* **1987**, *16*, 187–238.
- [43] a) S. H. Friedman, P. S. Ganapathi, Y. Rubin, G. L. Kenyon, *J. Med. Chem.* **1998**, *41*, 2424–2429; b) W. Qian, Y. Rubin, *Angew. Chem.* **1999**, *111*, 2504; *Angew. Chem. Int. Ed.* **1999**, *38*, 2356–2360.
- [44] J. Sauer, R. Sustmann, *Angew. Chem.* **1980**, *92*, 773–801; *Angew. Chem. Int. Ed. Engl.* **1980**, *19*, 779–807.
- [45] R. C. Haddon, *Science* **1993**, *261*, 1545–1550.
- [46] K. N. Houk, Y. Li, J. D. Evanseck, *Angew. Chem.* **1992**, *104*, 711–739; *Angew. Chem. Int. Ed. Engl.* **1992**, *31*, 682–708.
- [47] a) J. Mestres, M. Duran, M. Sola, *J. Phys. Chem.* **1996**, *100*, 7449–7454; b) A. Chikama, H. Fueno, H. Fujimoto, *J. Phys. Chem.* **1995**, *99*, 8541–8549.
- [48] B. R. Beno, Y. Rubin, K. N. Houk, unpublished results.
- [49] T. Kusukawa, W. Ando, *Angew. Chem.* **1996**, *108*, 1416–1418; *Angew. Chem. Int. Ed. Engl.* **1996**, *35*, 1315–1317.
- [50] a) A. K. Abdul-Sada, A. G. Avent, P. R. Birkett, H. W. Kroto, R. Taylor, D. R. M. Walton, *J. Chem. Soc. Perkin Trans. 1* **1998**, 393–395; b) P. R. Birkett, A. G. Avent, A. D. Darwish, I. Hahn, H. W. Kroto, G. J. Langley, J. Oloughlin, R. Taylor, D. R. M. Walton, *J. Chem. Soc. Perkin Trans. 2* **1997**, 1121–1125; c) A. K. Abdul-Sada, A. G. Avent, P. R. Birkett, A. D. Darwish, H. W. Kroto, R. Taylor, D. R. M. Walton, O. B. Woodhouse, *Chem. Commun.* **1998**, 307–308; d) A. G. Avent, P. R. Birkett, A. D. Darwish, H. W. Kroto, R. Taylor, D. R. M. Walton, *Chem. Commun.* **1997**, 1579–1580; e) P. R. Birkett, A. G. Avent, A. D. Darwish, H. W. Kroto, R. Taylor, D. R. M. Walton, *J. Chem. Soc. Perkin Trans. 2* **1997**, 457–461; f) A. G. Avent, P. R. Birkett, A. D. Darwish, H. W. Kroto, R. Taylor, *Tetrahedron* **1996**, *52*, 5235–5246.
- [51] For mechanistic aspects of the [3,3] sigmatropic rearrangement, see: a) R. K. Hill, in *Comprehensive Organic Synthesis, Vol. 5* (Eds.: B. M. Trost, I. Fleming), Pergamon, New York, **1991**, pp. 785–826; b) R. P. Lutz, *Chem. Rev.* **1984**, *84*, 205–247.